

Surfactant transport onto a foam film in the presence of surface viscous stress

Denny Vitasari^a, Paul Grassia^{b,c,*}, Peter Martin^d

^a*Department of Chemical Engineering, Universitas Muhammadiyah Surakarta,
Jl A Yani Tromol Pos 1 Pabelan Sukarta 57162, Indonesia*

^b*Department of Chemical and Process Engineering, University of Strathclyde,
James Weir Building, 75 Montrose St, Glasgow G1 1 XJ, UK*

^c*Departamento Ciencias Matemáticas y Físicas, Universidad Católica de Temuco,
Rudecindo Ortega 02950, Temuco, Chile*

^d*School of Chemical Engineering and Analytical Science, The Mill, The University of Manchester,
Oxford Road, Manchester M13 9PL, UK*

Abstract

Surfactant transport onto a foam film in the presence of surface viscosity has been simulated as a model for processes occurring during foam fractionation with reflux. A boundary condition is specified determining the velocity at the end of the film where it joins up with a Plateau border containing surfactant rich reflux material. The evolutions of surface velocity and surfactant surface concentration on the film are computed numerically using a finite difference method coupled with the material point method. Results are analysed both for low and high surface viscosities. Evolution is comparatively rapid when surface viscosity is low, but the larger the surface viscosity becomes, the slower the surface flow, and the lower the surfactant surface concentration on the film at any given time. For a large surface viscosity, the surface concentration of surfactant is maintained nearly uniform except at positions near the Plateau border where the velocity and surfactant concentration fields need to adjust to satisfy the boundary condition at the end of the film. The boundary condition imposed at the end of the film implies also that a drier foam (i.e. smaller radius of curvature of the Plateau border) leads to less surfactant transport onto the films. Moreover, the shorter the film length is, also the shorter the characteristic time for surfactant transport onto the film surface. Thinner films however give longer characteristic times for surfactant transport.

Keywords: Foam fractionation; Reflux; Marangoni effect; Interfacial viscosity; Surfactant transfer; Mathematical modelling

1. Introduction

Foam fractionation is an inexpensive and environmentally friendly separation process for recovering surface active compounds from dilute aqueous solutions [1]. The foam process is applied for separation of various materials including proteins [1–5], biosurfactants [6–10], microorganisms [11, 12], and other surface active materials [1]. Foam fractionation is usually performed in a fractionation column, gas being sparged from the bottom of the column to create bubbles which form a rising foam. The principle of the separation is

*Corresponding author

Email address: paul.grassia@strath.ac.uk (Paul Grassia)

by selective adsorption of a surface active material (hereafter called a ‘surfactant’) to the surfaces of gas bubbles that are moving towards the top of the column [13].

Some foam fractionation columns are equipped with reflux to increase separation efficiency [14–17] by enhancing the enrichment of the foamate. Reflux may be either internal or external [5, 16, 18]. Internal reflux proceeds by in situ bubble coalescence redistributing surfactant rich material onto films neighbouring those that have recently burst. External reflux (the particular situation we study here) proceeds by adding a portion of the collapsed foamate back to the top of the column: it flows down through the network of Plateau borders (channels along which three films meet) transporting surfactant to neighbouring films as it flows pasts them. This transport is driven by Marangoni stresses: surfactant-rich Plateau borders, which are fed by reflux material, have lower surface tensions than neighbouring surfactant-lean films that are yet to benefit from reflux.

This Marangoni-driven surfactant transfer process has been the subject of a recent study [19]. However that study neglected a potentially important interface science effect: Marangoni-driven flows on film surfaces may be opposed by surface viscous effects [20–22]. Indeed the surface viscosity of adsorbed monolayers plays a crucial role in the formation, stability and rheology of emulsions or foams as well as in the process of film coating, spraying, flotation and oil recovery [23]. Surface viscosity moreover determines [24] the velocity profile when surfactant solution flows along a Plateau border in a foam. When surface viscosity is **high**, the flow pattern within the Plateau border is mainly determined by the bulk viscosity with no slip on the walls of the border. However when surface viscosity is low, significant motion on the walls takes place.

Despite the effect that surface viscosity has upon surfactant flows, and despite the importance of surfactant flows to foam fractionation processes, we are not aware of any prior studies that have specifically looked at the role of surface viscosity upon fractionation performance. In an attempt to address this, the present study focuses on modelling the effects of surface viscosity specifically upon surfactant mass transfer during foam fractionation with reflux. The main focus here is not therefore on flow within Plateau borders [24], but rather on flow on films, as well as flow between Plateau borders and films. Our main finding is that surface viscosity reduces (possibly quite substantially) the rate of surfactant transfer onto a film, thereby reducing the efficiency of the reflux process during fractionation. The higher the surface viscosity of the surfactant, the longer the time that films must spend in contact with the Plateau borders in order that reflux material manages to transfer onto the films: this impacts on the residence time for which films must be present in the column. Should residence times turn out to be insufficient for transfer of a very high surface viscosity surfactant to occur, the fractionation process would need to be modified e.g. by changing column height and/or changing the rate at which bubbles are driven along the column.

This work is laid out as follows. Section 2 introduces the mathematical model of film surface velocity with surface viscosity, including the assumptions used and the boundary conditions assigned. **This same section also introduces the mathematical model governing surfactant concentration on the film.** Section 3 discusses the challenges involved in quantifying surface viscosity and the variability in reported measurement results. Section 4 presents simulation parameters **selected** for our model. The **numerical** solution **methodology** is presented in Section 5. The **numerical** results of the time evolution of surface velocity and surfactant surface concentration are discussed in Section 6. Conclusions are presented in Section 7.

2. Mathematical model of the surface velocity

Deformation of the surface of a foam film leads to surface stresses [20, 25]. Those surface stresses can be an elastic stress or viscous stress or both. The viscous stress can originate from shear deformation and dilational deformation **of the film surface itself**, while the elastic stress originates from dilation **of the film surface**, and is characterised by a Gibbs elasticity parameter. The **surface** shear and **surface** dilational viscous stresses (per unit strain rate) are characterized by constants called respectively surface shear viscosity and surface dilational viscosity. For a particular mode of surface deformation that involves specified amounts of both surface shear and dilation (as e.g. in the specified geometry to be considered below), these constants can be combined together into a single surface viscosity parameter.

A mathematical model of the velocity within the bulk of a foam film and on its surface is developed below: a 2-D bulk flow field and 1-D surface flow are considered (Figure 1). For simplicity, we study a 2-D bulk field rather than e.g. an axisymmetric one here. In dry foams at least, foam films tend to be polygonal rather than circular, so switching to an axisymmetric field would add complexity but still not be perfectly accurate geometrically.

This section is laid out as follows. Subsection 2.1 describes the assumptions taken to develop the model, while Subsection 2.2 introduces the equations **for surface velocity**. Subsection 2.3 presents **a key parameter influencing the model behaviour**, while Subsection 2.4 describes the boundary conditions **associated with the surface velocity profile**. **Finally Subsection 2.5 discusses the surfactant conservation equation, which coupled to the surface velocity profile, determines the rate of evolution of surfactant concentration.**

2.1. Assumptions of the model

The mathematical model of surface velocity in this study is developed based on the following assumptions:

- At initial time, the surface concentration of surfactant along the film is uniform.
- The surface concentration of surfactant on the Plateau border is fixed all the time to the value set by the reflux to the foam fractionation column. This is higher than the initial surface concentration on the film. **Whilst it is possible in principle to generalize to the case where the surfactant concentration in the Plateau borders gradually decreases as material is transferred across to the films, this is a complication we have chosen to ignore here. What matters for driving flow is the surfactant concentration difference between borders and films, and this concentration difference decreases with time as the film surfactant concentration rises, even when changes in the Plateau border concentration are ignored.**
- The liquid **in** the film is incompressible and Newtonian. The film **surface** is however viscoelastic, **supporting both surface viscous stress and elastic Marangoni stress**.
- The film is taken to be flat and has uniform thickness along its length [19, 26, 27]. Moreover liquid drainage from films is ignored, so film thicknesses are held constant with time. **These assumptions are mathematically convenient, as they greatly simplify the flow fields we need to compute. It should be mentioned however that foam films are known to develop non-uniform, dimpled shapes [28–30], whilst film drainage tends to oppose Marangoni-driven surfactant motion from surfactant-rich Plateau borders to surfactant-lean films [19].**

- The thickness of the film is much smaller than its length, consequently the associated Reynolds number, with length scale based on the film thickness, is very small [31] and a lubrication approximation is assumed [32–38].
- The Plateau border, which has a tricuspid shape, has a characteristic size that is intermediate between the film length and the film thickness, but may well contain rather more liquid than the exceedingly thin films.

The mathematical model for evolution of surfactant surface concentration (developed by [19] and to be employed **in what follows**) utilises the following additional assumptions.

- Films are sufficiently thin (or equivalently surfactant solubility is sufficiently low) that the surface excess of surfactant dominates any surfactant in solution in the bulk of the film. In other words, even if surfactant manages to diffuse from film surfaces across their bulk [33], the surfactant that is ‘lost’ from the surface is insignificant compared to the overall surfactant budget. **Recall also that film drainage is ignored from our model, as was stated previously. Were film drainage to be present however, any material that diffuses from the film surface to the film interior, would in principle be advected by the film drainage velocity field back towards the Plateau border, leading to quite a complex transport process overall that we choose to neglect here.**
- Marangoni-driven surfactant flows along surfaces are much faster than surfactant diffusion along surfaces.

2.2. Governing equations

The equation for the profile of surface velocity taking into account the surface viscosity is developed based on lubrication theory and driving Marangoni-stresses. The **equation governing the profile of the surface velocity (which can be obtained from a generalisation of a procedure outlined by [19], and which involves a straightforward balance between the viscous shear stress immediately below the surface and the gradient of surface elastic tension and surface viscous tension along the surface)** turns out to obey [39]:

$$u_s = \frac{\delta_0}{3\mu} \left[\frac{\partial \gamma}{\partial x} + \frac{\partial}{\partial x} \left(\mu_s \frac{\partial u_s}{\partial x} \right) \right] \quad (1)$$

where u_s is the surface velocity, x is the distance from the centre of the film along its length, δ_0 is the half thickness of the film, μ is the liquid viscosity, γ is the surface tension, μ_s is the surface viscosity.

We use a simple Gibbs elasticity model [40] to convert between surface tension γ and surfactant surface excess Γ :

$$d\gamma/d \ln \Gamma = -G \quad (2)$$

where G is a Gibbs parameter that we take to be a constant. This captures the tendency of γ to decrease as Γ increases, but represents nonetheless a considerable simplification of the true relation between γ and Γ (contrast e.g. the much more complicated relations in [41]). Equation (2) was used in [19] because it leads to a convenient linear relation between surfactant concentration gradient and surfactant flux, giving (in the absence of surface viscosity) a linear partial differential equation for the spatio-temporal evolution of Γ . We adopt the same model here to facilitate comparison between results with and without surface viscosity.

We deduce

$$u_s = \frac{\delta_0}{3\mu} \left[\frac{\partial}{\partial x} \left(-G \ln \frac{\Gamma}{\Gamma_{Pb}} \right) + \frac{\partial}{\partial x} \left(\mu_s \frac{\partial u_s}{\partial x} \right) \right] \quad (3)$$

where Γ_{Pb} is the (fixed) surface excess of surfactant on the surface of the Plateau border. This is larger than the surface excess on the film (Γ or Γ_{F0} initially at time $t = 0$). The right hand side of equation (3) represents a Kelvin-type viscoelastic model for a foam film surface, and corresponds to what was done by [40]. We note however that there are competing Maxwell-type viscoelastic models in the literature [42, 43].

A dimensional analysis was carried out upon equation (3) and results in:

$$u'_s = -\frac{1}{3} \frac{\partial \ln \Gamma'}{\partial x'} + \frac{\delta'_0 \bar{\mu}_s}{3} \frac{\partial^2 u'_s}{\partial x'^2}. \quad (4)$$

where $u'_s = u_s \mu / G \delta'_0$ is the dimensionless surface velocity, $\delta'_0 = \delta_0 / L$ is the dimensionless half film thickness, δ_0 is the half film thickness, L is half of the film length, $x' = x / L$ is the dimensionless distance from the centre of the film along its length, $\Gamma' = \Gamma / \Gamma_{Pb}$ is the dimensionless surface excess of surfactant and $\bar{\mu}_s = \mu_s / \mu L$ is the dimensionless surface viscosity. The dimensionless surface viscosity is the reciprocal of the surface mobility parameter identified in previous studies [24, 44].

2.3. Role of the parameter $\delta'_0 \bar{\mu}_s$

The parameter $\delta'_0 \bar{\mu}_s$ is important in equation (4) since it determines the effect of surface viscosity upon the system (an estimated value for this parameter will be provided shortly). If $\delta'_0 \bar{\mu}_s$ is small, the effect of surface viscosity is weak, and the equation of the surface velocity profile can be simplified as follows:

$$u'_s = -\frac{1}{3} \frac{\partial \ln \Gamma'}{\partial x'} \quad (5)$$

which indicates that film surface velocity is driven by Marangoni effects [19], any surface viscous effects being neglected.

Note a significant difference between equation (4) and (5). Whereas the former equation is a second order differential equation in space (and so the velocity field can only be determined given suitable boundary conditions, which we will consider in Subsection 2.4), the latter gives the velocity u'_s directly once the surfactant concentration field Γ' vs x' is known. There is no guarantee in this case that boundary conditions on u'_s will be met.

This then indicates that even in the limit of small $\delta'_0 \bar{\mu}_s$, the velocity field might need to deviate away from equation (5) in boundary layers. Equation (4) implies that the characteristic thickness of these boundary layers must be order $(\delta'_0 \bar{\mu}_s)^{1/2}$, since for a boundary layer on that length scale, the nominally ‘small’ surface viscous term in equation (4) namely $\frac{1}{3} \delta'_0 \bar{\mu}_s \partial^2 u'_s / \partial x'^2$ becomes comparable with the other two terms in that equation. Further discussion about these boundary layers can be found in the appendix.

On the other hand, if $\delta'_0 \bar{\mu}_s$ is very large, there is balance between the Marangoni effect and surface viscosity, and it turns out that $u'_s \ll 1$. In this limit it is convenient to rescale the velocity, i.e. to define u''_s such that $u''_s = \delta'_0 \bar{\mu}_s u'_s$ (or equivalently $u''_s = u_s \bar{\mu}_s / GL$) so that equation (4) becomes

$$\frac{3u''_s}{\delta'_0 \bar{\mu}_s} = -\frac{\partial \ln \Gamma'}{\partial x'} + \frac{\partial^2 u''_s}{\partial x'^2}. \quad (6)$$

As a result, for $\delta'_0 \bar{\mu}_s \gg 1$, we can simplify into the following equation:

$$\partial^2 u_s'' / \partial x'^2 = \partial \ln \Gamma' / \partial x'. \quad (7)$$

Equation (7) indicates that the total film tension which consists of the Gibbs-Marangoni and surface viscosity contributions is spatially uniform when $\delta'_0 \bar{\mu}_s$ is very large. **It turns out that the solution of equation (7) for u_s'' can be expressed in terms of an integral over $\ln \Gamma'$ as is described in the appendix. Nonetheless equation (7), like equations (4) and (6), can however only be solved uniquely given suitable boundary conditions.**

The determination of the boundary condition is presented in the following subsection.

2.4. Boundary conditions

The surface velocity u'_s must vanish midway along the film (i.e. at $x' = 0$) on symmetry grounds. In addition, due to symmetry on the Plateau border, the value of u'_s must also fall to zero at the ‘symmetry point’ of a tricuspoid Plateau border (see Figure 2). The ‘symmetry point’ is the midpoint of the curved section of each tricuspoid arc. Since each of the tricuspoid curves subtends an arc $\pi/3$, the angle subtended between the cusp and the symmetry point is $\pi/6$, making the distance (measured along the film) between the cusp and the midpoint be $L'_{Pb} = a'\pi/6$, where $a' = a/L$ is the dimensionless radius of curvature of the Plateau border and a is the radius of curvature of the Plateau border. **We can also think of the parameter a' as being connected with the liquid fraction of the foam [45]: the volume of liquid contained in the Plateau borders around a bubble relative to the bubble volume itself scales proportional to a'^2 .**

We can take the (dimensionless) distance from the centre of the film to the ‘symmetry point’ of a tricuspoid Plateau border (measured along the surface) as $1 + a'\pi/6$. On symmetry grounds, the velocity component along the surface accelerates away from the the symmetry point where it vanishes (or equivalently decelerates towards the symmetry point). Surface viscosity couples the motion of nearby points to one another: given the comparatively small size of the Plateau border (compared to the film length), points towards the end of the film may well be influenced by the fact that the symmetry point of the Plateau border remains stationary. In particular, if the surface viscosity is large, the fact that the velocity component must be zero at the symmetry point will couple back to the film, keeping the surface flow very small especially at the end of the film. **Moreover the drier the foam (i.e. the smaller the value of a') the more strongly the end of the film is coupled to the stationary Plateau border symmetry point, and the less the permitted surfactant transfer onto the end of the film.**

The surface of the tricuspoid Plateau border is of course a complicated 2-D shape. As a simplifying approximation, we unfold it into a 1-D line. By ‘uncurling’ the surface of the tricuspoid Plateau border, we simplify the geometry as well as the mathematics but still capture the essential physics of the flow accelerating away from the symmetry point (or equivalently decelerating towards the symmetry point).

Two boundary conditions are required to solve the differential equation (4). One boundary condition is at $x' = 0$ where we have $u'_s|_{x'=0} = 0$. The other boundary condition is taken at $x' = 1$ by imposing the constraint at the symmetry point of a tricuspoid Plateau border and supposing that u'_s is nearly linear in x' over the domain $1 < x' < 1 + a'\pi/6$ (i.e. the surface velocity decelerates uniformly between the end of the film and the symmetry point of the Plateau border). Therefore, the boundary condition at the end of the film

near the Plateau border is as follows:

$$\left. \frac{\partial u'_s}{\partial x'} \right|_{x'=1} = \frac{0 - u'_s|_{x'=1}}{a'\pi/6} \quad (8)$$

rearranging to:

$$u'_s|_{x'=1} + \frac{a'\pi}{6} \left. \frac{\partial u'_s}{\partial x'} \right|_{x'=1} = 0. \quad (9)$$

The velocity boundary condition at the end of film in equations (8) and (9) is shifted to $x' = 1$ instead of at the symmetry point itself at $x' = 1 + a'\pi/6$. The reason for shifting the boundary condition in this fashion is that the fluid flow and the surfactant mass transfer model that we analyse considers only the domain of the film (i.e. $0 < x' < 1$) without any detailed model for the Plateau border ($1 < x' < 1 + a'\pi/6$). The detailed flow field in the Plateau border itself is very complex – with flow changing direction within the border – and it is beyond the scope of this study.

Having a boundary condition at $x' = 1$ is also convenient when solving the mass conservation equation for surfactant (since Γ' only needs to be computed in the domain $0 < x' < 1$) and one can simply assume that surfactant coverage on the Plateau border is fixed. This follows because typically, the bulk of the liquid in a foam is in the Plateau borders (meaning that the Plateau border surfaces can continually be replenished by surfactant arriving from the interior of the borders). This does not contradict the notion of the surfactant being nominally ‘low solubility’ which only requires that surfactant be present primarily as surface excess on the length scale of the (exceedingly thin) films.

According to equation (9) the velocity at the end of the film, $u'_s|_{x'=1}$ can be affected by the parameter a' , which is normally quite a small parameter (being the ratio between the length scale of the Plateau border cross section and the length scale along the films).

Recall however that when the parameter $\delta'_0 \bar{\mu}_s \ll 1$, the velocity field both near $x' = 0$ and near $x' = 1$ is potentially affected by boundary layers, the relevant boundary layer size being order $(\delta'_0 \bar{\mu}_s)^{1/2}$. In practice no boundary layer arises near $x' = 0$, the reason being that $\partial \ln \Gamma' / \partial x'$ vanishes there on symmetry grounds, and equation (5) then predicts the correct boundary condition $u'_s|_{x'=0} = 0$ even with vanishing surface viscosity. A boundary layer does however arise near $x' = 1$. In fact, very different behaviour is expected according to whether the boundary layer size of order $(\delta'_0 \bar{\mu}_s)^{1/2}$ is lesser or greater than the distance $\pi a'/6$ to the symmetry point of the Plateau border. The reasons for this are as follows.

In the case where the boundary layer size is much less than the distance to the border symmetry point, i.e. $(\delta'_0 \bar{\mu}_s)^{1/2} \ll \pi a'/6$, the boundary layer is effectively unaware of the constraint imposed by the Plateau border symmetry point, and so a comparatively large velocity is permitted at $x' = 1$ transferring surfactant from Plateau border to film. On the other hand, when $(\delta'_0 \bar{\mu}_s)^{1/2} \gg \pi a'/6$, the boundary layer on the film is well aware of the constraint arising from the Plateau border symmetry point, and (as a result) the surfactant velocity at the end of the film is substantially reduced. Further details of this situation can be found in the appendix.

This completes our model of the surface velocity field on a foam film in the presence of surface viscosity. This surfactant velocity field then advects the surfactant causing the surfactant concentration to change: this process is considered in the next subsection.

2.5. Evolution of surfactant concentration

As in previous work [19], we adopt the following conservation equation for the evolution of surfactant surface concentration or excess (which is itself a special case for a flat

interface of a more general equation considered by [46])

$$\partial\Gamma'/\partial t' + \partial(\Gamma' u'_s)/\partial x' = 0. \quad (10)$$

Here t' is a dimensionless time related to dimensional time t via $t' = tG\delta'_0/L\mu$. Clearly equation (10) is a partial differential equation for Γ' to be solved along with the ordinary differential equation (4) governing u'_s . The technique for solving this equation will be discussed later on in Section 5, but for the moment we just make some brief remarks.

In the limit when $\delta'_0\bar{\mu}_s \gg 1$, we have already discussed how we can rescale dimensionless velocity (with rescaled velocity u''_s equal to $\delta'_0\bar{\mu}_s u'_s$). In a similar fashion we can rescale time, with rescaled time t'' defined as $t'' = t'/(\delta'_0\bar{\mu}_s)$, implying that $t'' = tG/\mu_s$. The form of equation (10) then remains unchanged provided we replace t' by t'' and u'_s by u''_s . Remember also (as commented in Subsection 2.3) that in the limit as $\delta'_0\bar{\mu}_s \gg 1$, the velocity field u''_s can be obtained in terms of an integral of $\ln \Gamma'$. If this is substituted into the surfactant conservation equation we have an integro-differential equation for $\ln \Gamma'$.

Whether we adopt the differential equation formulation of equation (10) (for finite $\delta'_0\bar{\mu}_s$) or the integro-differential equation formulation (for $\delta'_0\bar{\mu}_s \gg 1$) we need to supply initial and boundary conditions for dimensionless surfactant concentration Γ' . Initially the surfactant concentration is assumed to be uniform, $\Gamma' = \Gamma'_{F0}$ where Γ'_{F0} is a dimensionless constant (being the ratio between the dimensional concentrations Γ_{F0} and Γ_{Pb} respectively on the film and Plateau border). Here Γ'_{F0} is smaller than unity, since in the process of foam fractionation with reflux, comparatively surfactant-lean films contact comparatively surfactant-rich Plateau borders. The boundary condition meanwhile is that the dimensionless surfactant concentration at the point $x' = 1$ at the end of the film satisfies $\Gamma'|_{x'=1} = 1$ for all times $t' > 0$. In other words the dimensional surfactant concentration at the end of the film matches the surfactant concentration on the Plateau border. Note that (as has already been mentioned in Subsection 2.4) at the midpoint of the film $x' = 0$ a symmetry condition $\partial\Gamma'/\partial x'|_{x'=0} = 0$ also applies, but we do not need to impose this explicitly: it arises naturally from the symmetries of the governing equations.

This completes our formulation of the model for evolution of surfactant concentration. However in order to compute with the model we require values of model parameters, in particular values for the relevant surface rheological material properties. Unfortunately however these are not always readily obtained (as we explain in the next section).

3. Variability of measurements of surface viscosity

Measuring surface viscoelastic properties is very challenging since those properties are affected by environmental contamination [47]. Moreover, it is not always easy to distinguish between surface elasticity and surface viscosity [47], and, as a possible consequence it has been observed that different experimental methods to determine the surface viscosity result in measured values of surface viscosity differing by orders of magnitude [47–49]. Furthermore foam fractionation (our target application) is often employed as a technique for purifying proteins, but proteins can exist in many conformational states at surfaces [50], each state having different viscoelastic properties. Indeed the conformational state (and hence the viscoelastic properties) can change during the course of an experiment.

In this study we will use as a ‘base case’ a value for surface viscosity of bovine serum albumin (BSA) together with a cosurfactant propylene glycol alginate (PGA) as reported by [40]. We note however that for the common surfactant SDS the particular measurement technique of [40] determined surface viscosity values 5 orders of magnitude higher than

measurements on SDS performed by other authors [49]. Hence it is possible to speculate that the surface viscosity reported by [40] for BSA/PGA could be likewise too high.

The study of [40] also provided our ‘base case’ value of the **half** film thickness δ_0 . **That** study ignored film drainage, **whereas** a fully drained ‘common black’ film (**half** thickness denoted δ_{cb}) would have a thickness orders of magnitude smaller than our base case thickness value.

We already commented (Subsection 2.3) how the effect of surface viscosity **appears** as a product $\delta'_0 \bar{\mu}_s$, the parameter δ'_0 being dimensionless **half** film thickness and $\bar{\mu}_s$ being dimensionless surface viscosity. The effect of **possibly** having a dimensionless surface viscosity orders of magnitude smaller than our ‘base case’ **is** achieved analogously **in what follows** by **reducing the dimensionless film thickness, thereby** replacing the non-draining film of [40] by a much thinner **one that is substantially closer to a common black film**.

4. Parameters for simulation

Typical parameter values for the simulation are presented in Table 1 while the relevant dimensionless parameters are presented in Table 2.

All parameters except the values of Γ_{Pb} , Γ_{F0} , δ_{cb} , δ_0 and a were taken from [40] using protein BSA together with a cosurfactant PGA, both at concentration of 4.0 g L^{-1} . The value of a was estimated as presented in [19], while the value of δ_{cb} was taken from [45]. The values of Γ_{Pb} , Γ_{F0} are estimates, taken as lower than the maximum surface excess Γ_{max} of BSA which was reported in a study by [51] to be $\Gamma_{max} = 5 \times 10^{-8} \text{ mol m}^{-2}$. We reiterate these are base-case parameter values and variations about the base case will be considered in the simulations.

The **quantity** $\delta'_0 \bar{\mu}_s$ is the key parameter to determine the effect of surface viscosity upon the system. Using the base-case parameters presented in Table 1, the value of that key parameter is $\delta'_0 \bar{\mu}_s = 3.5 \pm 1.4$. However, **as already mentioned** there is a lot of uncertainty associated with this parameter, with the possibility of much smaller values being relevant. **Under such circumstances**, it is useful to understand how the system behaves in the limiting cases of small and large values of this parameter. This is achieved in Section 6, starting first of all with small $\delta'_0 \bar{\mu}_s$ and then progressing onto large $\delta'_0 \bar{\mu}_s$.

In the first instance we have elected to access small $\delta'_0 \bar{\mu}_s$ values, via keeping $\bar{\mu}_s$ fixed (at the base case value of 886 given in Table 2), whilst reducing δ'_0 , specifically taking the δ'_0 value to be 6×10^{-5} , intermediate between δ'_{cb} (namely 3×10^{-6} , the smallest allowed value as mentioned in Table 2), and the base case δ'_0 (which is 4×10^{-3} in Table 2). The resulting value of $\delta'_0 \bar{\mu}_s$ is now 5.4×10^{-2} and so is significantly smaller than unity. One consequence of reducing film thickness (it is now 66 times smaller than the base case) is that we also increase the characteristic time scale shown in Table 1 by the same factor: instead of being 0.134 s, it is now close to 9 s.

To access a large $\delta'_0 \bar{\mu}_s$ we have decided to retain the same δ'_0 value as just discussed above (namely 6×10^{-5}) but to increase $\bar{\mu}_s$ by two orders of magnitude (from the base case $\bar{\mu}_s$ value of 886, to a new value of 8.86×10^4). The resulting $\delta'_0 \bar{\mu}_s$ is now slightly larger than the base case value quoted in Table 1, specifically $\delta'_0 \bar{\mu}_s$ now equals 5.4 instead of the base case value 3.5.

The parameter **ranges** used specifically in these small and large $\delta'_0 \bar{\mu}_s$ computations are presented in Table 3. The base case a' value is $a' = 0.1$. Most of our computations are done for this value, but a small number of them will be done for $a' = 0.25$ corresponding to a wetter foam. The parameter Γ'_{F0} is fixed at 0.5, i.e. only half as much surfactant concentration on the film surfaces initially as on the Plateau borders.

We reiterate that the key parameter here is $\delta'_0\bar{\mu}_s$ which according to Subsection 2.3 affects the velocity field u'_s and/or u''_s , and this in turn influences the evolution of Γ' . Our main aim here is to determine how $\delta'_0\bar{\mu}_s$ affects surfactant transport by solving the governing equations numerically. Additional insight into the role of this $\delta'_0\bar{\mu}_s$ parameter can however be gained by obtaining analytical expressions for u'_s and/or u''_s for given simple analytical forms of Γ' : these are taken up in the appendix. The simple analytical forms of Γ' might only apply for a restricted set of times, since Γ' is continually evolving. The velocity fields one determines are nevertheless instructive as the appendix explains.

5. Numerical solution technique

The numerical solution technique for equation (10) follows a material point method used by [19]. We outline the method briefly here, but readers should refer to [19] for more details. Discrete material points are distributed along the foam film surface and also (in the specific case of a foam fractionation column with reflux) where the film meets a surfactant rich Plateau border. Velocities of each material point are computed, in the present case incorporating surface viscosity by a finite difference method applied to equation (4). The material point positions change on every time step, leading to uneven spatial intervals over time. To keep the spatial intervals even, a bookkeeping operation is applied at the end of every time step to restore equal width intervals: this then recovers second order spatial accuracy for the numerical scheme. The mechanism of the bookkeeping operation is similar to the one reported in the previous study [19]. Moreover the temporal accuracy of the numerical simulation is improved using a predictor-corrector method namely Heun's method [52, 53].

The system is discretised [54] into $I+1$ spatial (material) points, i.e. I spatial intervals, and N time steps. Values of I ranged between 200 and 250, whilst values of N ranged between 10000 and 20000. In the case of a small $\delta'_0\bar{\mu}_s$, specifically $\delta'_0\bar{\mu}_s = 5.4 \times 10^{-2}$, we chose $I = 250$ giving a spatial interval $\Delta x' = 4 \times 10^{-3}$. Moreover we chose $N = 20000$ and integrated to $t' = 2$ (corresponding to a time step $\Delta t' = 10^{-4}$). In the case of a large $\delta'_0\bar{\mu}_s$, specifically $\delta'_0\bar{\mu}_s = 5.4$, we chose $I = 200$ giving a spatial interval $\Delta x' = 5 \times 10^{-3}$. Moreover we chose $N = 10000$ and integrated to a rescaled time $t'' = 20$ (corresponding to a time step $\Delta t'' = 2 \times 10^{-3}$).

In addition to the above, we performed a number of convergence tests, including doubling the number of spatial steps and/or halving the number of time of steps, and looking at the root mean square of differences in predicted Γ' vs x' profiles at either $t' = 2$ or $t'' = 20$. This resulted in a root mean square difference of 2×10^{-3} (or less) comparing coarser vs finer spatial grids, and a root mean square difference of 10^{-4} (or less) comparing coarser vs finer temporal grids.

Recall (from Subsection 2.5, and also the appendix) that for $\delta'_0\bar{\mu}_s \gg 1$ we can replace the differential equation (10) by an integro-differential equation. We solved this on a fixed (Eulerian) grid with $I = 200$ spatial intervals and $N = 20000$ time steps out to $t'' = 20$.

Typical run times for our programs were on the order of a few minutes. Results from these programs are presented in Section 6 below.

6. Evolution of surface velocity and surfactant surface concentration

In what follows numerical results are presented for velocity and surfactant surface concentration fields. Bearing in mind the different behaviours expected between the cases $\delta'_0\bar{\mu}_s \ll 1$ and $\delta'_0\bar{\mu}_s \gg 1$, we treat these two cases in turn. Subsection 6.1 presents

the evolution of surface velocity and surfactant surface concentration in the case where $\delta'_0\bar{\mu}_s$ is significantly smaller than unity, specifically $\delta'_0\bar{\mu}_s = 5.4 \times 10^{-2}$. Subsection 6.2 deals with the case where $\delta'_0\bar{\mu}_s$ is significantly larger than unity, specifically $\delta'_0\bar{\mu}_s = 5.4$. Subsection 6.3 discusses the effects of considering different film lengths.

6.1. Evolution in the case where $\delta'_0\bar{\mu}_s \ll 1$

Data shown in this subsection have $\delta'_0\bar{\mu}_s = 5.4 \times 10^{-2}$, $a' = 0.1$ and $\Gamma'_{F0} = 0.5$.

Surface velocity profiles are presented in Figure 3. At early times, velocity is near zero far from $x' = 1$, as velocity profiles are sharply peaked near $x' = 1$. The maximum surface speed occurs very slightly to the left of $x' = 1$ however, due to a need to meet the velocity boundary condition at $x' = 1$. At later times the velocity distributions are more spread out and the peak speeds are less.

The corresponding surface concentration of surfactant is presented in Figure 4. Over time the surfactant concentration grows and the surfactant concentration profile becomes increasingly spread out. For comparison the evolution of surfactant surface concentration in the absence of surface viscosity is presented in Figure 5. Comparing the surface concentrations calculated in the presence of surface viscosity and in its absence, it appears that surfactant transport onto the foam film is slower in the case with surface viscosity. At early time, the growth of surfactant surface concentration obtained using the model with surface viscosity is **actually** much slower than that obtained using the model without surface viscosity. The mass of surfactant transferred in fact grows like square root of time in the absence of surface viscosity [19], but only linearly in time in the presence of surface viscosity (**because surface viscosity keeps the film velocity finite even for an arbitrarily sharp gradient of surfactant concentration**). At later time, the relative difference of surface concentration obtained using those two models becomes smaller.

The spatially-averaged surfactant surface concentration over time with surface viscosity can be compared with that in the case without surface viscosity and the result is presented in Figure 6. In the case without surface viscosity, at early time, the rate of accumulation of surfactant on the surface of the film is faster than that in the case with surface viscosity. This is shown by the steep increase of surface concentration at early time for the case without surface viscosity. In the case with surface viscosity, this early time growth is moderated by the surface viscous effect. At later time, the rate of accumulation of surfactant on the surface of the film **slows down**, and the predictions in the presence and absence of surface viscosity are similar (albeit with slightly less surfactant transferred in the former case).

6.2. Evolution in the case where $\delta'_0\bar{\mu}_s \gg 1$

In the case where $\delta'_0\bar{\mu}_s \gg 1$, it is convenient to rescale the dimensionless velocity and time as described in Subsections 2.3 and 2.5. The rescaled equations are solved **either via finite differences with the material point method (see Subsection 6.2.1) or via an integro-differential equation (see Subsection 6.2.2)**. Subsection 6.2.3 considers analytic approximations to the solutions, whilst Subsection 6.2.4 contrasts large vs small $\delta'_0\bar{\mu}_s$.

6.2.1. Solution using finite difference method for the case of $\delta'_0\bar{\mu}_s \gg 1$

This subsection presents results for the case where $\delta'_0\bar{\mu}_s = 5.4$, $a' = 0.1$ and $\Gamma'_{F0} = 0.5$.

The profiles of surface velocity obtained are presented in Figure 7. **It is clear that gradients** of surface velocity are nearly spatially uniform away from $x' = 1$. **This is in fact the behaviour expected (see the appendix)**. At early time, the magnitude of u''_s

(in this region away from $x' = 1$) grows. If the width of the region near $x' = 1$ over which the surfactant concentration deviates from uniformity grows, the magnitude of $\partial u_s''/\partial x'$ (and hence of u_s'' itself) outside this region also grows, **again as predicted in the appendix**. At later times however, the magnitude of $\partial u_s''/\partial x'$ decays, since gradients of surface concentration eventually decay as surfactant accumulates on the film surface, implying that **the Marangoni forces which ultimately drive the flow field become weaker**.

Near the end of the film, the surface velocity profile deviates from a straight line to satisfy the $x' = 1$ boundary condition. The magnitude of surface velocity right at the end of the film $x' = 1$ turns out to be a decreasing function of time (see the inset in Figure 7).

Profiles of surfactant surface concentration are presented in Figure 8. As anticipated in **the appendix**, the surface concentration of surfactant is uniformly distributed along the film except at positions near the Plateau border. The uniform concentration region does seem to shrink in size between times $t'' = 0$ and $t'' = 4$ but then starts growing again.

We can rationalise this observation as follows. The non-uniform concentration region near the Plateau border tends to invade the uniform region further away when there is more surfactant flux entering the film from the Plateau border at $x' = 1$ than entering the uniform region slightly to the left of $x' = 1$. Conversely the uniform region tends to expel the non-uniform region back towards the Plateau border when the surfactant flux entering the film from the Plateau border at $x' = 1$ is less than that entering the uniform region slightly further to the left.

The magnitude of the surfactant flux is the product $\Gamma'|u_s''|$, remembering $u_s'' < 0$ here. As we move leftwards from $x' = 1$, the value of Γ' falls, and this tends to reduce the surfactant flux, in turn giving a tendency for the non-uniform concentration region to grow and the uniform region to shrink. Counterbalancing this, again moving leftwards starting from $x' = 1$, the magnitude of $|u_s''|$ grows moving across the non-uniform concentration region towards the uniform one, tending to increase the surfactant flux: this favours shrinkage of the non-uniform region at the expense of growth of the uniform one. Concentration gradients in the non-uniform region must sharpen as the region itself shrinks¹.

When the non-uniform concentration region is highly compact, the change in $|u_s''|$ is negligible moving leftward from $x' = 1$ across the non-uniform region. The dominant tendency affecting the spatial variation of the surfactant flux is therefore that due to the change in Γ' , and hence the non-uniform concentration region grows at the expense of the uniform one. As the size of the non-uniform concentration region grows however, more substantial changes in $|u_s''|$ can occur moving leftward from $x' = 1$ across the non-uniform region up to the edge of the uniform one. These changes in $|u_s''|$ now dominate the spatial variation of the surfactant flux. This then permits the uniform concentration region to grow at the expense of the non-uniform one.

6.2.2. Calculation of surfactant surface concentration via an integro-differential equation

We now describe results obtained via the integro-differential equation as detailed in the appendix. As in Subsection 6.2.1, we have $a' = 0.1$ and $\Gamma'_{F0} = 0.5$, but we now have formally $\delta'_0\bar{\mu} \rightarrow \infty$ instead of $\delta'_0\bar{\mu} = 5.4$ as was the case for Figure 7–Figure 8.

¹Note that this mechanism sustaining sharp gradients of surfactant concentration really only relies on relative variations in u_s'' exceeding relative variations in Γ' , and does not demand large $\delta'_0\bar{\mu}_s$, even though we have discussed it in that particular context. An analogous mechanism could also be active in the case of small $\delta'_0\bar{\mu}_s$, as the sharpness of the surfactant concentration gradients near $x' = 1$ in Figure 4 (compared to Figure 5) indeed suggests.

Integro-differential equation surfactant concentration profiles results are presented in Figure 9. They are remarkably similar to those of Figure 8 **even though** one set of results (finite difference) was determined for $\delta'_0 \bar{\mu}_s = 5.4$ and the other set (integro-differential equation) formally for $\delta'_0 \bar{\mu}_s \rightarrow \infty$. **This close similarity is also reflected in the spatially-averaged surfactant surface concentration plotted vs time in Figure 10. To quantify the differences in the spatially-averaged data between the finite $\delta'_0 \bar{\mu}_s$ cases compared to the case where $\delta'_0 \bar{\mu}_s \rightarrow \infty$, we evaluated the root mean square difference of the spatially-averaged data between times $t'' = 0$ and $t'' = 20$. This root mean square difference was 0.0013 for $\delta'_0 \bar{\mu}_s = 5.4$, rising to 0.0031 for $\delta'_0 \bar{\mu}_s = 2.7$ and to 0.0168 for $\delta'_0 \bar{\mu}_s = 0.54$.**

6.2.3. Comparison with approximate analytic solution

Using the assumption of near uniform surfactant surface concentration over (almost all of) the film, the evolution of surfactant surface concentration in the uniform region can be predicted using **equation (A.10) given in the appendix.**

In Figure 11, predictions from equation (A.10) are compared with the finite difference and integro-differential equation computations. In this figure, the data is only presented up to two units of time to show the agreement of the results of the three methods for calculation of Γ' at $x' = 0$. At very early times equation (A.10) agrees with the finite difference and/or integro-differential equation results. At later time, the predictions obtained using equation (A.10) deviate from the two other methods. This is because equation (A.10) assumes an arbitrarily abrupt jump in surfactant surface concentration at the end of the film, whereas in reality the concentration changes over a thin but finite region. **Note that according to the numerical predictions the growth rate of surfactant surface concentration at $x' = 0$ increases over time as the region where the profile of Γ' vs x' departs from uniformity grows, and this must be associated with increases in the magnitude of the surface strain rate $|\partial u''_s / \partial x'|$ in those parts of the domain where Γ' remains uniform.**

6.2.4. Comparison of large and small surface viscosity cases

Our data for large $\delta'_0 \bar{\mu}_s$ have been expressed in terms a rescaled time t'' instead of t' . Given that $t' = \delta'_0 \bar{\mu}_s t''$, **clearly** our large $\delta'_0 \bar{\mu}_s$ data consider time scales much longer than those studied with a smaller surface viscosity parameter. To effect a comparison between the small and large $\delta'_0 \bar{\mu}_s$ data, we convert the latter back into the original t' scaling. The result for spatially-averaged surfactant surface concentration is presented in Figure 12. It is clear that the rate of surfactant transport onto the film surface is much slower for large surface viscosity compared to the small surface viscosity case.

Just how slowly this large $\delta'_0 \bar{\mu}_s$ case evolves for the current set of parameter values can be appreciated by referring to Figure 10 which indicates that the surfactant concentration on the film has only proceeded about half way to equilibrium with the Plateau border even by $t'' = 10$ (or equivalently by $t' = 54$ since $\delta'_0 \bar{\mu}_s = 5.4$ here). Remember from Section 4 that 1 unit of dimensionless time t' corresponds to roughly 9 s (this is longer than the scale 0.134 s quoted in Table 1 because we are assuming a substantially smaller film thickness as Section 4 explains). It follows that, in a foam fractionation column operated with reflux, to equilibrate a high surface viscosity film with surfactant rich reflux material in Plateau borders, we may need to ensure that the contact time between the film and the Plateau borders is hundreds of seconds long². Strategies for increasing this contact time

²In fact the reason that such a long time scale results here is that we have chosen a value of $\bar{\mu}_s = 8.86 \times 10^4$ which is 100 times bigger than the base case value quoted in Table 1. Each unit of rescaled

(or equivalently for increasing the film residence time in the fractionation column) could be to increase the column height and/or operate at a lower air flow rate.

6.3. Effect of varying film length

Changing the film length (correlating with a change in bubble size) affects the characteristic time scale for moving surfactant onto the film. A shorter film has a shorter characteristic time, given (in dimensional form) by $L^2\mu/(G\delta_0)$ as per Table 1.

In the limit $\delta'_0\bar{\mu}_s \ll 1$ at least, being the limit for which the characteristic time scale $L^2\mu/(G\delta_0)$ is relevant, a decrease in L should lead to a very substantial decrease in (dimensional) time to achieve surfactant mass transfer. Not only do the Marangoni forces become stronger with decreasing L , but also the distance over which surfactant needs to travel onto the film is less. Although the mass transfer time scale can be reduced significantly by reducing the film length, in the small $\delta'_0\bar{\mu}_s$ limit it is already comparatively short compared to other time scales of interest, e.g. residence time of foam films in the fractionation column [19]. Therefore, there is unlikely to be any requirement to reduce it further. Reducing bubble size may have other beneficial effects for foam fractionation though, e.g. increasing specific surface area, and thereby increasing the total amount of adsorbed surfactant present in the fractionation column.

When $\delta'_0\bar{\mu}_s \gg 1$, the characteristic time scale changes (see Subsection 2.5) to μ_s/G (in dimensional form). This is independent of the film length. In other words, for a decrease in film length L , surface viscosity placing more limitations on surface motion on short film, is offset (as far as evolution of surfactant concentration is concerned) by the shorter distance over which surfactant must travel. The only residual effect is from the parameter a' increasing as L decreases (which should give more rapid transfer – constraints on surfactant motion imposed by the Plateau border are less relevant as the film shrinks relative to the Plateau border). This then corresponds to the case of a wetter foam.

In this study the result of calculation using a shorter film ($L = 2 \times 10^{-3}$ m, corresponding to $a' = 0.25$) is compared with that using a longer film ($L = 5 \times 10^{-3}$ m, the value of L contemplated in Table 1, corresponding to $a' = 0.1$). Profiles of surfactant surface concentration for a film with $L = 2 \times 10^{-3}$ m are presented in Figure 13 for various values of $t'' = Gt/\mu_s$. These have been computed with the integro-differential equation approach (formally $\delta'_0\bar{\mu}_s \rightarrow \infty$) so that the parameter $\delta'_0\bar{\mu}_s$ has ceased to play any role whatsoever, and the only effect of changing film length L is the residual effect of changing a' .

It is shown that at any time t'' , the surfactant surface concentration obtained in the calculation using a shorter film in Figure 13 is larger than that obtained using a longer film given in Figure 9. For further comparison, the spatially-averaged surfactant surface concentration for the short film ($L = 2 \times 10^{-3}$ m) is compared with that for a longer film ($L = 5 \times 10^{-3}$ m). Results are presented in Figure 14. Again it is apparent that for a shorter film the rate of surfactant accumulation is faster than that for a longer film.

When determining time scales for mass transfer, potentially even more important than introducing high surface viscosities and/or varying film length, is considering different possible film thicknesses. The nominal time scale for mass transfer 0.134 s quoted in Table 1 (neglecting surface viscosity and taking $L = 5 \times 10^{-3}$ m) assumed the particular half film thickness quoted in that table namely $\delta_0 = 20 \times 10^{-6}$ m (or equivalently $\delta'_0 = 4 \times 10^{-3}$ quoted in Table 2). The much smaller value of half film thickness actually used

dimensionless time t'' (and we are interested in at least 10 such units) corresponds to a physical time μ_s/G or equivalently $\bar{\mu}_s\mu L/G$, where according to Table 1, $\mu L/G = 5.3 \times 10^{-4}$ s.

in our calculations ($\delta'_0 = 6 \times 10^{-5}$) implies a substantially longer characteristic time scale, on the order of 9 s as noted in Section 4. A further reduction of half film thickness (by another order of magnitude down to the half thickness of a common black film δ_{cb} quoted in Table 1) implies yet another order of magnitude increase in the mass transfer time scale. Ironically this increased time scale is associated with lesser importance of surface viscosity (as this depends on the parameter $\delta'_0 \bar{\mu}_s$ which decreases with falling film thickness). Knowledge of film drainage rates which govern film thicknesses is very important for determining the rate of mass transfer.

What is counterintuitive here is that increasing surface viscosity at a given film thickness leads to very long mass transfer times (as Subsection 6.2.4 indicates). However reducing film thickness at fixed surface viscosity, also increases the mass transfer time, even though it diminishes the relative importance that surface viscosity plays.

7. Conclusions

Simulation of surfactant transport onto a foam film in the presence of surface viscous stress has been carried out. The simulation describes phenomena occurring during the process of foam fractionation with reflux being used to purify a surfactant, and in particular how those phenomena are affected by the interfacial rheology of the surfactant. The foam film surface is assumed to be viscoelastic and to be characterised by a Gibbs elasticity and a surface viscosity parameter, both treated crudely as being independent of surfactant surface concentration.

The base case parameter set for the simulation was taken from experimental data reported in the literature using the protein bovine serum albumin (BSA) together with cosurfactant propylene glycol alginate (PGA). Reflecting uncertainty in possible parameter values, the parameter set we actually explored varied widely about the base case. The simulation computes via finite differences the surface velocity distribution in the presence of surface viscous stress. In order to determine the surface velocities, an approximation was used, whereby the Plateau border was ‘uncurled’ onto a straight line, and the surface velocity on the border itself was assumed to vary linearly with distance from the symmetry point of the border, but with non-linear variation permitted on the adjacent film. The surface velocities advect surfactant, and cause the surface concentration (or surface excess) of surfactant to evolve, and this was also computed using a material point method.

The evolution of the system was affected by the surface viscosity represented in the form of dimensionless parameter $\delta'_0 \bar{\mu}_s$.

In computations with $\delta'_0 \bar{\mu}_s \ll 1$, velocity profiles are initially quite sharply peaked, but at a later time, the profiles of surface velocity are less sharp since the surfactant surface concentration spreads out more evenly on the film surface, which results in more spread out but weaker Marangoni stress. At any given time, the surfactant surface concentration in the presence of surface viscosity is lower than that without surface viscosity. The rate of surfactant transport is thereby affected by the surface viscosity parameter.

For a large surface viscosity, $\delta'_0 \bar{\mu}_s \gg 1$, and in the special case where surfactant concentration is nearly uniform along the film, the surface velocity profile is proportional to the distance from the centre of the film except at positions near the Plateau border, where the velocity field needs to adjust to satisfy the boundary condition at the end of film. As a consequence, the surfactant surface concentration remains distributed almost evenly at positions far from the Plateau border. In the large $\delta'_0 \bar{\mu}_s$ limit, the profile of surfactant surface concentration can also be simulated using an integro-differential equation. Simulation results using the integro-differential equation agree with those using

the finite difference method. It is found that the velocity scale is greatly slowed down in the high surface viscosity limit (scaling now inversely with the surface viscosity) **and the time scale for evolution of the surfactant concentration is correspondingly increased.**

Finally when a shorter film length is applied in the calculation, the characteristic time scale for surfactant transport is likewise shorter.

We would expect the trends identified above to be reflected in the rate of enrichment seen in a fractionation column operated with reflux, e.g. slower enrichment with higher surface viscosity, slower enrichment in a very dry foams, but faster enrichment with smaller bubbles. Foam film thickness is another important factor determining the mass transfer rate associated with reflux-induced Marangoni flow. Ironically reducing film thickness reduces the relative importance of surface viscosity, but increases the time scale for mass transfer. Computing these mass transfer time scales is important for designing fractionation processes: the residence time of foam films in the fractionation column must be sufficient to achieve the required transfer. **Indeed an experimental study measuring the effect of foam film residence time on the performance of a foam fractionation column operated with reflux for a comparatively high surface viscosity surfactant seems to be a promising avenue for future research.**

Acknowledgements

DV acknowledges financial support provided by Directorate General of Higher Education Republic of Indonesia and Universitas Muhammadiyah Surakarta Indonesia. PG acknowledges sabbatical stay funding CONICET Argentina res. no. 2218/13 **and from CONICYT Chile folio 80140040.**

Appendix A. Velocity fields for instantaneous distributions of Γ'

In the main text we computed the fields u'_s and Γ' coupled together. Specifically given an instantaneous distribution of Γ' vs x' one can compute u'_s vs x' , and thereby how Γ' vs x' evolves with time. Generally speaking, the field Γ' vs x' can be quite complex, and this leads to a complex field for u'_s vs x' and hence a complex evolution of Γ' .

If however one assumes a comparatively simple field for Γ' vs x' at a particular instant in time, it becomes possible to solve for u'_s vs x' analytically. These analytic solutions are of course only valid at one instant in time (because Γ' vs x' is itself evolving) but nonetheless useful insights can be gained from them. We treat the small $\delta'_0 \bar{\mu}_s$ and large $\delta'_0 \bar{\mu}_s$ cases separately.

Appendix A.1. Small $\delta'_0 \bar{\mu}_s$ case

The particular instant in time that we will consider is time $t' = 0$, for which we know that $\Gamma' = \Gamma'_{F0}$ for $x' < 1$ and $\Gamma' = 1$ for $1 < x' \leq 1 + \frac{\pi}{6}a'$. Here recall Γ'_{F0} is a constant smaller than unity, so we have low surfactant concentration on the film, and higher surfactant concentration on the Plateau border.

It is useful to define a quantity a'_{crit} as

$$a'_{crit} = \frac{6}{\pi} \sqrt{\frac{\delta'_0 \bar{\mu}_s}{3}}. \quad (\text{A.1})$$

The physical interpretation of this quantity will be given shortly.

The surface velocity for $x' \leq 1$ can be described by the following equation:

$$u'_s = -\frac{\ln(1/\Gamma'_{F0})}{3\sqrt{\delta'_0\bar{\mu}_s/3}(1+a'_{crit}/a')} \exp\left(\frac{-1+x'}{\sqrt{\delta'_0\bar{\mu}_s/3}}\right). \quad (\text{A.2})$$

Since $\delta'_0\bar{\mu}_s \ll 1$ this solution clearly has the character of a boundary layer, the length scale of the boundary layer being $\sqrt{\delta'_0\bar{\mu}_s/3}$ (which is indeed an order $(\delta'_0\bar{\mu}_s)^{1/2}$ quantity as anticipated in the main text): once x' moves a distance of $\sqrt{\delta'_0\bar{\mu}_s/3}$ away from $x' = 1$, it is clear that the magnitude of u'_s decays, and in fact when $\delta'_0\bar{\mu}_s \ll 1$, the boundary condition that $u'_s = 0$ at $x' = 0$ is satisfied with only negligible, exponentially small, error. In effect the solution already decays over such a short distance to the left of $x' = 1$ that, with negligible error, we can push the $u'_s = 0$ boundary condition from $x' = 0$ all the way to $x' \rightarrow -\infty$.

Moreover for any $x' < 1$, our solution (A.2) clearly satisfies the governing equation (4) (because by assumption Γ' is uniform with x' when $x' < 1$). Furthermore it can be verified that boundary condition (9) is satisfied. As $x' \rightarrow 1$ from below, the value of $\partial u'_s/\partial x'$ can be obtained readily from equation (A.2). At $x' = 1$ however, equation (4) requires that there be an abrupt change in $\partial u'_s/\partial x'$, itself equal to the imposed abrupt change or ‘jump’ in $\ln \Gamma'$ divided by $\delta'_0\bar{\mu}_s$. Hence the value of $\partial u'_s/\partial x'$ immediately to the right of $x' = 1$ can be deduced, and verification of the boundary condition (9) follows.

Note an important property of equation (A.2). When $a' \gg a'_{crit}$ (i.e. when $\frac{\pi}{6}a' \gg \sqrt{\delta'_0\bar{\mu}_s/3}$), u'_s at $x' = 1$ approaches a value $-\frac{1}{3}(\delta'_0\bar{\mu}_s/3)^{-1/2} \ln(1/\Gamma'_{F0})$ which is insensitive to the value of a' . The $\frac{\pi}{6}a'$ distance between the end of the film and the symmetry point of the Plateau border is now so large compared to the characteristic decay distance of the velocity boundary layer ($\sqrt{\delta'_0\bar{\mu}_s/3}$ or equivalently $\frac{\pi}{6}a'_{crit}$) that in effect the velocity field is unconstrained by the presence of the Plateau border symmetry point. When $a' \ll a'_{crit}$ on the other hand, the magnitude of u'_s is greatly reduced, becoming a factor a'/a'_{crit} smaller than the aforementioned unconstrained velocity value. This greatly reduced velocity then leads to a reduced flux of surfactant from the Plateau border onto the film. Thus we deduce the following physical interpretation of the parameter a'_{crit} , namely a'_{crit} is a critical value of the parameter a' , such that for $a' \gg a'_{crit}$ the velocity field is unconstrained by the requirement for velocity to fall to zero at the Plateau border symmetry point, whereas if $a' \ll a'_{crit}$ the velocity field is strongly constrained by this requirement.

This completes our discussion of the case of small $\delta'_0\bar{\mu}_s$. The case of large $\delta'_0\bar{\mu}_s$ behaves very differently as we shall see in the next subsection.

Appendix A.2. Large $\delta'_0\bar{\mu}_s$ case

In the case of large $\delta'_0\bar{\mu}_s$ it is convenient to rescale the velocity, defining $u''_s = \delta'_0\bar{\mu}_s u'_s$. The velocity field is now governed by equation (7), the solution of which is

$$u''_s = -\left[\int_0^{x'} \ln\left(\frac{1}{\Gamma'}\right) dx' - \frac{x'}{1+a'\pi/6} \int_0^1 \ln\left(\frac{1}{\Gamma'}\right) dx' \right]. \quad (\text{A.3})$$

It is easy to check by direct substitution confirms that this satisfies equations (7) and (9).

Note that equation (A.3) is generically true in the limit $\delta'_0\bar{\mu}_s \gg 1$ regardless of how Γ' varies with x' . Using (A.3), the spatio-temporal evolution of Γ' can be computed (via the

surfactant conservation equation)

$$\begin{aligned} \frac{\partial \Gamma'}{\partial t''} = & \left[\int_0^{x'} \ln \left(\frac{1}{\Gamma'} \right) dx' - \frac{x'}{1 + a'\pi/6} \int_0^1 \ln \left(\frac{1}{\Gamma'} \right) dx' \right] \frac{\partial \Gamma'}{\partial x'} \\ & + \left[\ln \left(\frac{1}{\Gamma'} \right) - \frac{1}{1 + a'\pi/6} \int_0^1 \ln \left(\frac{1}{\Gamma'} \right) dx' \right] \Gamma'. \end{aligned} \quad (\text{A.4})$$

This is the integro-differential equation to which we refer extensively in the main text, and which we solve in Subsection 6.2.2.

Note however that owing to equation (A.3) we can already deduce quite a lot about the velocity field u'_s even without solving equation (A.4) in detail. For example for $x' = 1$ we obtain the following equation:

$$u''_s|_{x'=1} = -\frac{a'\pi/6}{1 + a'\pi/6} \int_0^1 \ln \left(\frac{1}{\Gamma'} \right) dx', \quad (\text{A.5})$$

this velocity $u''_s|_{x'=1}$ then governing the surfactant flux from Plateau border to film. Clearly the closer Γ' is to unity, the nearer $u''_s|_{x'=1}$ becomes to zero.

Yet more deductions about the velocity field can be made by employing a simplification, namely assuming uniform surfactant surface concentration away from the end of the film ($x' = 1$). This is dealt with in the next subsection.

Appendix A.3. Surface velocity: Uniform surfactant concentration away from $x' = 1$

Suppose that the surfactant concentration field Γ' is uniform with a value Γ'_0 except possibly in a thin region near $x' = 1$. This is certainly true in the initial state at early times (and in fact $\Gamma'_0 = \Gamma'_{F0}$ in that case). However the data in Figure 8 and Figure 9 indicate it remains roughly true even as time proceeds, although Γ'_0 varies with time.

Equation (A.3) then indicates that to a good approximation

$$u''_s \approx -\frac{x'a'\pi/6}{1 + a'\pi/6} \ln \left(\frac{1}{\Gamma'_0} \right). \quad (\text{A.6})$$

Therefore the derivative of equation (A.6) can be presented as follows:

$$\frac{\partial u''_s}{\partial x'} \approx -\frac{a'\pi/6}{1 + a'\pi/6} \ln \left(\frac{1}{\Gamma'_0} \right). \quad (\text{A.7})$$

This $\partial u''_s/\partial x'$ applies for the overwhelming majority of the length of the film. However in the thin region near $x' = 1$ the value of $\partial u''_s/\partial x'$ is rather different. In fact at $x' = 1$ equation (9) and equation (A.6) imply the following equation:

$$\left. \frac{\partial u''_s}{\partial x'} \right|_{x'=1} \approx \frac{1}{1 + a'\pi/6} \ln \left(\frac{1}{\Gamma'_0} \right). \quad (\text{A.8})$$

It is shown that outside the thin region near $x' = 1$, $\partial u''_s/\partial x'$ is a factor of $a'\pi/6$ smaller than (and of opposite sign to) $\partial u''_s/\partial x'$ at $x' = 1$. Therefore, there is an obvious asymmetry in the graph of u''_s vs x' with a gradual slope outside the thin region and a sharper slope inside the thin region. This asymmetry is clearly seen in Figure 7. Note also that u''_s is an order a' quantity, or equivalently (converting back to the original scaling) u'_s is order $a'/(\delta'_0 \bar{\mu}_s)$. Thus, the surface velocity u'_s can be decreased **not only** by increasing $\delta'_0 \bar{\mu}_s$ but

also by decreasing a' . In other words, the drier the foam (i.e. smaller a'), the lower the velocity at the edge of the film, and the less mass transfer from Plateau border to film.

Appendix A.4. Time evolution of (near uniform) surfactant concentration

In the case where Γ' is close to Γ'_0 (apart from a very thin region near $x' = 1$), the fact that equations (A.6)–(A.7) suggest a near uniform strain rate in the film has important implications for mass transfer. Specifically the near uniform strain rate drives a near uniform rate of change of surfactant concentration, in turn ensuring that the surfactant concentration field (whilst changing in time) remains close to spatially uniform (being then consistent with the assumptions under which equations (A.6)–(A.7) were derived).

An ordinary differential equation for the time evolution of Γ'_0 can be derived as follows:

$$\frac{\partial \Gamma'_0}{\partial t''} \approx \frac{a'\pi/6}{1 + a'\pi/6} \ln\left(\frac{1}{\Gamma'_0}\right) \Gamma'_0. \quad (\text{A.9})$$

Integration of equation (A.9) results in the following equation:

$$\Gamma'_0 \approx \exp\left(-\ln\left(\frac{1}{\Gamma'_{F0}}\right) \exp\left(-\frac{t'' a'\pi/6}{1 + a'\pi/6}\right)\right), \quad (\text{A.10})$$

where we have used the condition that $\Gamma'_0 = \Gamma'_{F0}$ as $t'' \rightarrow 0$.

Equation (A.10) gives the evolution of surfactant surface concentration outside a thin region near $x' = 1$. It is clear that $\Gamma'_0 \rightarrow \Gamma'_{F0}$ if $t'' \ll 1/(a'\pi/6)$, however $\Gamma'_0 \rightarrow 1$ if $t'' \gg 1/(a'\pi/6)$. This prediction for Γ'_0 relies of course on the assumption that the surfactant surface concentration is nearly spatially uniform.

There is of course a thin region near $x' = 1$ where Γ' deviates from the spatially uniform value Γ'_0 , since necessarily $\Gamma' \rightarrow 1$ at $x' = 1$. This non-uniform concentration region grows with time at least for small t'' (as Figure 8 and Figure 9 make apparent). This leads to a reduction in the value of the term $\int_0^1 \ln(1/\Gamma') dx'$ within equation (A.3). The term $\int_0^{x'} \ln(1/\Gamma') dx'$ within that same equation is however unaffected provided x' is chosen within the domain where Γ' is spatially uniform with the value Γ'_0 . The implication is that the magnitude of $\partial u''_s / \partial x'$ (which is itself uniform within the spatially uniform concentration region) grows as the spatially non-uniform region grows. This higher strain rate in turn causes Γ'_0 to grow more quickly than equations (A.9)–(A.10) predict, and this is evident in Figure 11. The velocity difference across the spatially non-uniform region (which is zero when the spatially non-uniform region is arbitrarily thin) must also grow as the spatially non-uniform region grows and the spatially uniform region shrinks. Increasing this velocity difference may however arrest the shrinkage of the spatially non-uniform region (see Subsection 6.2.1).

References

- [1] D. Linke, H. Zorn, B. Gerken, H. Parlar, R. G. Berger, Laccase isolation by foam fractionation – New prospects of an old process, *Enzyme and Microbial Technology* 40 (2007) 273–277.
- [2] L. Du, V. Loha, R. Tanner, Modeling a protein foam fractionation process, *Applied Biochemistry and Biotechnology* 84–86 (2000) 1087–1099.

- [3] D. Linke, R. G. Berger, Foaming of proteins: New prospects for enzyme purification processes, *Journal of Biotechnology* 152 (2011) 125–131.
- [4] B. M. Gerken, A. Nicolai, D. Linke, H. Zorn, R. G. Berger, H. Parlar, Effective enrichment and recovery of laccase C using continuous foam fractionation, *Separation and Purification Technology* 49 (2006) 291–294.
- [5] L. Brown, G. Narsimhan, P. C. Wankat, Foam fractionation of globular proteins, *Biotechnology and Bioengineering* 36 (9) (1990) 947–959.
- [6] J. B. Winterburn, A. B. Russell, P. J. Martin, Characterisation of HFBII biosurfactant production and foam fractionation with and without antifoaming agents, *Applied Microbiology and Biotechnology* 90 (2011) 911–920.
- [7] J. B. Winterburn, A. B. Russell, P. J. Martin, Integrated recirculating foam fractionation for the continuous recovery of biosurfactant from fermenters, *Biochemical Engineering Journal* 54 (2011) 132–139.
- [8] D. A. Davis, H. C. Lynch, J. Varley, The application of foaming for the recovery of surfactin from *B. subtilis* ATCC 21332 cultures, *Enzyme and Microbial Technology* 28 (2001) 346–354.
- [9] C.-Y. Chen, S. C. Baker, R. C. Darton, Continuous production of biosurfactant with foam fractionation, *Journal of Chemical Technology & Biotechnology* 81 (12) (2006) 1915–1922.
- [10] C.-Y. Chen, S. C. Baker, R. C. Darton, Batch production of biosurfactant with foam fractionation, *Journal of Chemical Technology & Biotechnology* 81 (12) (2006) 1923–1931.
- [11] K. Schügerl, Recovery of proteins and microorganisms from cultivation media by foam flotation, in: *New Products and New Areas of Bioprocess Engineering*, Springer, Berlin, Heidelberg, 2000, pp. 191–233.
- [12] K. H. Bahr, K. Schügerl, Recovery of yeast from cultivation medium by continuous flotation and its dependence on cultivation conditions, *Chemical Engineering Science* 47 (1) (1992) 11–20.
- [13] R. Lemlich, Adsorptive bubble separation methods: Foam fractionation and allied techniques, *Industrial and Engineering Chemistry* 60 (10) (1968) 16–29.
- [14] R. Lemlich, Principles of foam fractionation, in: E. S. Perry (Ed.), *Progress in Separation and Purification*, Interscience, New York, 1968, pp. 1–56.
- [15] R. Lemlich, E. Lavi, Foam fractionation with reflux, *Science* 134 (3473) (1961) 191.
- [16] P. J. Martin, H. M. Dutton, J. B. Winterburn, S. Baker, A. B. Russell, Foam fractionation with reflux, *Chemical Engineering Science* 65 (12) (2010) 3825–3835.
- [17] P. Stevenson, G. J. Jameson, Modelling continuous foam fractionation with reflux, *Chemical Engineering and Processing: Process Intensification* 46 (12) (2007) 1286–1291.

- [18] P. Stevenson, X. Li, G. M. Evans, A mechanism for internal reflux in foam fractionation, *Biochemical Engineering Journal* 39 (3) (2008) 590–593.
- [19] D. Vitasari, P. Grassia, P. Martin, Surfactant transport onto a foam lamella, *Chemical Engineering Science* 102 (2013) 405–423.
- [20] L. E. Scriven, Dynamics of a fluid interface. Equation of motion for Newtonian surface fluids, *Chemical Engineering Science* 12 (2) (1960) 98–108.
- [21] L. E. Scriven, C. V. Sternling, On cellular convection driven by surface-tension gradients: Effects of mean surface tension and surface viscosity, *Journal of Fluid Mechanics* 19 (1964) 321–340.
- [22] I. B. Ivanov, K. D. Danov, K. P. Ananthapadmanabhan, A. Lips, Interfacial rheology of adsorbed layers with surface reaction: On the origin of the dilatational surface viscosity, *Advances in Colloid and Interface Science* 114–115 (2005) 61–92.
- [23] J. T. Petkov, K. D. Danov, N. D. Denkov, R. Aust, F. Durst, Precise method for measuring the shear surface viscosity of surfactant monolayers, *Langmuir* 12 (11) (1996) 2650–2653.
- [24] R. A. Leonard, R. Lemlich, A study of interstitial liquid flow in foam. Part I. Theoretical model and application to foam fractionation, *AIChE J.* 11 (1) (1965) 18–25.
- [25] M. van den Tempel, J. Lucassen, E. H. Lucassen-Reynders, Application of surface thermodynamics to Gibbs elasticity, *Journal of Physical Chemistry* 69 (6) (1965) 1798–1804.
- [26] P. S. Stewart, S. H. Davis, Dynamics and stability of metallic foams: Network modeling, *Journal of Rheology* 56 (2012) 543–574.
- [27] P. S. Stewart, S. H. Davis, Self-similar coalescence of clean foams, *Journal of Fluid Mechanics* 722 (2013) 645–664.
- [28] S. P. Frankel, K. J. Mysels, On the dimpling during the approach of two interfaces, *Journal of Physical Chemistry* 66 (1) (1962) 190–191.
- [29] J. L. Joye, G. J. Hirasaki, C. A. Miller, Dimple formation and behavior during axisymmetrical foam film drainage, *Langmuir* 8 (12) (1992) 3083–3092.
- [30] J. L. Joye, G. J. Hirasaki, C. A. Miller, Asymmetric drainage in foam films, *Langmuir* 10 (9) (1994) 3174–3179.
- [31] L. Y. Yeo, O. K. Matar, E. S. P. de Ortiz, G. F. Hewitt, The dynamics of Marangoni-driven local film drainage between two drops, *Journal of Colloid and Interface Science* 241 (1) (2001) 233–247.
- [32] I. B. Ivanov, Effect of surface mobility on the dynamic behavior of thin liquid films, *Pure and Applied Chemistry* 52 (5) (1980) 1241–1262.
- [33] I. B. Ivanov, D. S. Dimitrov, Thin film drainage, in: I. B. Ivanov (Ed.), *Thin Liquid Films: Fundamentals and Applications*, Marcel Dekker Incorporated, New York, Basel, 1988, pp. 382–489.

- [34] P. A. Kralchevsky, K. D. Danov, N. D. Denkov, Chemical physics of colloid systems and interfaces, in: K. S. Birdi (Ed.), Handbook of Surface and Colloid Chemistry, 3rd Edition, Taylor & Francis, Boca Raton, 1997, pp. 333–477.
- [35] S. I. Karakashev, D. S. Ivanova, Z. K. Angarska, E. D. Manev, R. Tsekov, B. Radoev, R. Slavchov, A. V. Nguyen, Comparative validation of the analytical models for the Marangoni effect on foam film drainage, Colloids and Surfaces A: Physicochemical and Engineering Aspects 365 (2010) 122–136.
- [36] B. P. Radoëv, D. S. Dimitrov, I. B. Ivanov, Hydrodynamics of thin liquid films. Effect of the surfactant on the rate of thinning, Colloid and Polymer Science 252 (1974) 50–55.
- [37] O. Reynolds, On the theory of lubrication and its application to Mr. Beauchamp Tower’s experiments, including an experimental determination of the viscosity of olive oil, Philosophical Transactions of the Royal Society of London 177 (1886) 157–234.
- [38] T. T. Traykov, I. B. Ivanov, Hydrodynamics of thin liquid films. Effect of surfactants on the velocity of thinning of emulsion films, International Journal of Multiphase Flow 3 (1977) 471–483.
- [39] D. Vitasari, Adsorption and transport of surfactant/protein onto a foam lamella within a foam fractionation column with reflux, PhD thesis, University of Manchester (2014).
- [40] M. Durand, H. A. Stone, Relaxation time of the topological T1 process in a two-dimensional foam, Physical Review Letters 97 (22) (2006) 226101.
- [41] D. Vitasari, P. Grassia, P. Martin, Simulation of dynamics of adsorption of mixed protein-surfactant on a bubble surface, Colloids and Surfaces A: Physicochemical and Engineering Aspects 438 (2013) 63–76.
- [42] F. Boury, T. Ivanova, I. Panaiotov, J. E. Proust, A. Bois, J. Richou, Dynamic properties of poly(DL-lactide) and polyvinyl-alcohol monolayers at the air-water and dichloromethane water interfaces, Journal of Colloid and Interface Science 169 (1995) 380–392.
- [43] I. Panaiotov, D. S. Dimitrov, L. Terminassiansaraga, Dynamics of insoluble monolayers. 2. Viscoelastic behavior and Marangoni effect for mixed protein phospholipid films, Journal of Colloid and Interface Science 72 (1979) 49–53.
- [44] A. M. Kraynik, Foam drainage, Tech. Rep. SAND83-0844, Sandia National Laboratories, Albuquerque, New Mexico, USA (1983).
- [45] D. Weaire, S. Hutzler, The Physics of Foams, Oxford University Press, Oxford, New York, 1999.
- [46] H. A. Stone, A simple derivation of the time-dependent convective-diffusion equation for surfactant transport along a deforming interface, Physics of Fluids A 2 (1990) 111–112.

- [47] Y. Tian, R. G. Holt, R. E. Apfel, Investigation of liquid surface rheology of surfactant solutions by droplet shape oscillations: Experiments, *Journal of Colloid and Interface Science* 187 (1) (1997) 1–10.
- [48] P. Stevenson, Remarks on the shear viscosity of surfaces stabilised with soluble surfactants, *Journal of Colloid and Interface Science* 290 (2) (2005) 603–606.
- [49] Z. A. Zell, A. Nowbahar, V. Mansard, L. G. Leal, S. S. Deshmukh, J. M. Mecca, C. J. Tucker, T. M. Squires, Surface shear inviscidity of soluble surfactants, *Proceedings of the National Academy of Sciences* 111 (10) (2014) 3677–3682.
- [50] R. Miller, V. B. Fainerman, M. E. Leser, M. Michel, Kinetics of adsorption of proteins and surfactants, *Current Opinion in Colloid and Interface Science* 9 (5) (2004) 350–356.
- [51] V. B. Fainerman, E. H. Lucassen-Reynders, R. Miller, Description of the adsorption behaviour of proteins at water/fluid interfaces in the framework of a two-dimensional solution model, *Advances in Colloid and Interface Science* 106 (1–3) (2003) 237–259.
- [52] N. W. Loney, *Applied Mathematical Methods for Chemical Engineers*, CRC Press, Boca Raton, 2001.
- [53] W. H. Press, S. A. Teukolsky, W. T. Vetterling, B. P. Flannery, *Numerical Recipes: The Art of Scientific Computing*, 3rd Edition, Cambridge University Press, Cambridge, 2007.
- [54] B. Embley, P. Grassia, Viscous froth simulations with surfactant mass transfer and Marangoni effects: Deviations from Plateau’s rules, *Colloids and Surfaces A: Physicochemical and Engineering Aspects* 382 (2011) 8–17.

Table 1: Parameters for simulation of surfactant transport onto a foam film incorporating surface viscosity taken from [40]. The value of surface viscosity μ_s as well as the error bar is the one observed by [40]. Some other experiments (e.g. [49]) suggest much smaller values of μ_s than have been reported by [40]. Depending upon the extent of film drainage, the half film thickness δ_0 can also be chosen much smaller than the value quoted (and many of our calculations do in fact select a substantially smaller value). Note that the characteristic Marangoni time scale differs somewhat from that reported by [19] as we are assuming a different surfactant with a different bulk liquid viscosity and different Gibbs parameter [40]. Moreover the characteristic Marangoni time scale is specific to the quoted half film thickness δ_0 . The time scale is proportional to the reciprocal of δ_0 .

Parameters	Symbol	Value	Unit
Characteristic ‘Marangoni’ time scale (equivalent to one unit of dimensionless time)	$L^2\mu/(G\delta_0)$	0.134	s
Initial half film thickness	δ_0	20×10^{-6}	m
Half thickness of common black film	δ_{cb}	15×10^{-9}	m
Half film length	L	5×10^{-3}	m
Liquid viscosity	μ	7×10^{-3}	Pa s
Surface viscosity	μ_s	$31 \pm 12 \times 10^{-3}$	Pa m s
Surfactant surface excess on the Plateau border	Γ_{Pb}	3×10^{-8}	mol m ⁻²
Initial surfactant surface excess on the film	Γ_{F0}	1.5×10^{-8}	mol m ⁻²
Radius of curvature of the Plateau border	a	5×10^{-4}	m
Surface tension on the Plateau border	γ_{Pb}	55×10^{-3}	N m ⁻¹
Gibbs parameter	G	$65 \pm 12 \times 10^{-3}$	N m ⁻¹

Table 2: Base case dimensionless parameters for the simulation of surfactant onto a foam film incorporating surface viscosity. The values were determined based primarily on [40].

Parameters	Symbol	Definition	Value
Dimensionless initial half film thickness	δ'_0	δ_0/L	4×10^{-3}
Dimensionless half thickness of common black film	δ'_{cb}	δ_{cb}/L	3×10^{-6}
Dimensionless radius of curvature of Plateau border	a'	a/L	0.1
Dimensionless surface viscosity	$\bar{\mu}_s$	$\mu_s/\mu L$	$8.86 \pm 3.4 \times 10^2$
Dimensionless initial surfactant surface excess	Γ'_{F0}	Γ_{F0}/Γ_{Pb}	0.5

Table 3: Range of the dimensionless parameters used in the simulation of surfactant transport onto a foam film incorporating surface viscosity. The value of δ'_0 is set intermediate between the smallest possible value ($\delta'_{cb} = 3 \times 10^{-6}$ quoted in Table 2) and the base case value δ'_0 value (4×10^{-3} again quoted in Table 2). The value of $\bar{\mu}_s$ and a' are set at least as large as the base case values (which are $\bar{\mu}_s = 886$ and $a' = 0.1$ respectively).

Parameters	Symbol	Range
Dimensionless initial half film thickness	δ'_0	6×10^{-5}
Dimensionless surface viscosity	$\bar{\mu}_s$	$886-8.86 \times 10^{-4}$
Dimensionless viscosity parameter	$\delta'_0 \bar{\mu}_s$	$5.4 \times 10^{-2}-5.4$
Dimensionless radius of curvature of Plateau border	a'	0.10–0.25

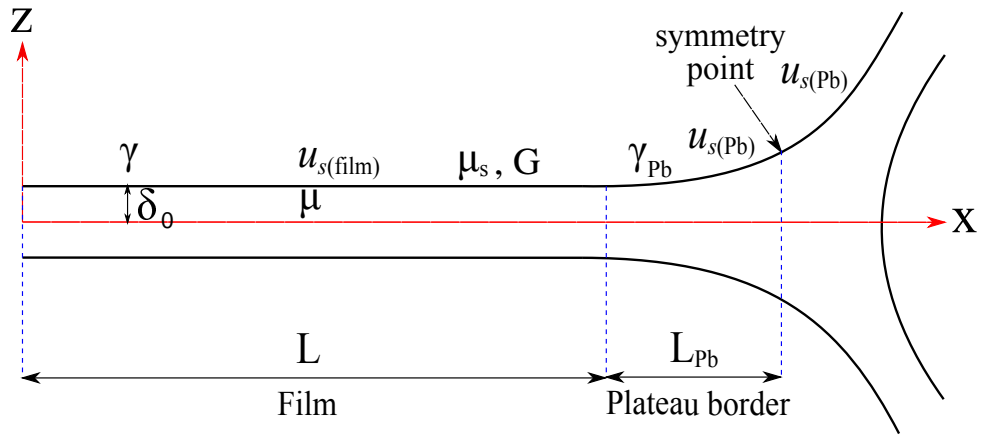


Figure 1: Two-dimensional slice of half of a foam film and an adjacent Plateau border. The film half length is L and the half film thickness is δ_0 , the Plateau border length (measured along the border to its symmetry point) is L_{Pb} , surface tensions are γ_{Pb} and γ on the surface of the Plateau border and on the surface of the film respectively, surface and bulk viscosity are μ_s and μ respectively, Gibbs elasticity on the film is G , surface velocities are $u_{s(Pb)}$ and $u_{s(\text{film})}$ on the surface of the Plateau border and on the surface of the film respectively.

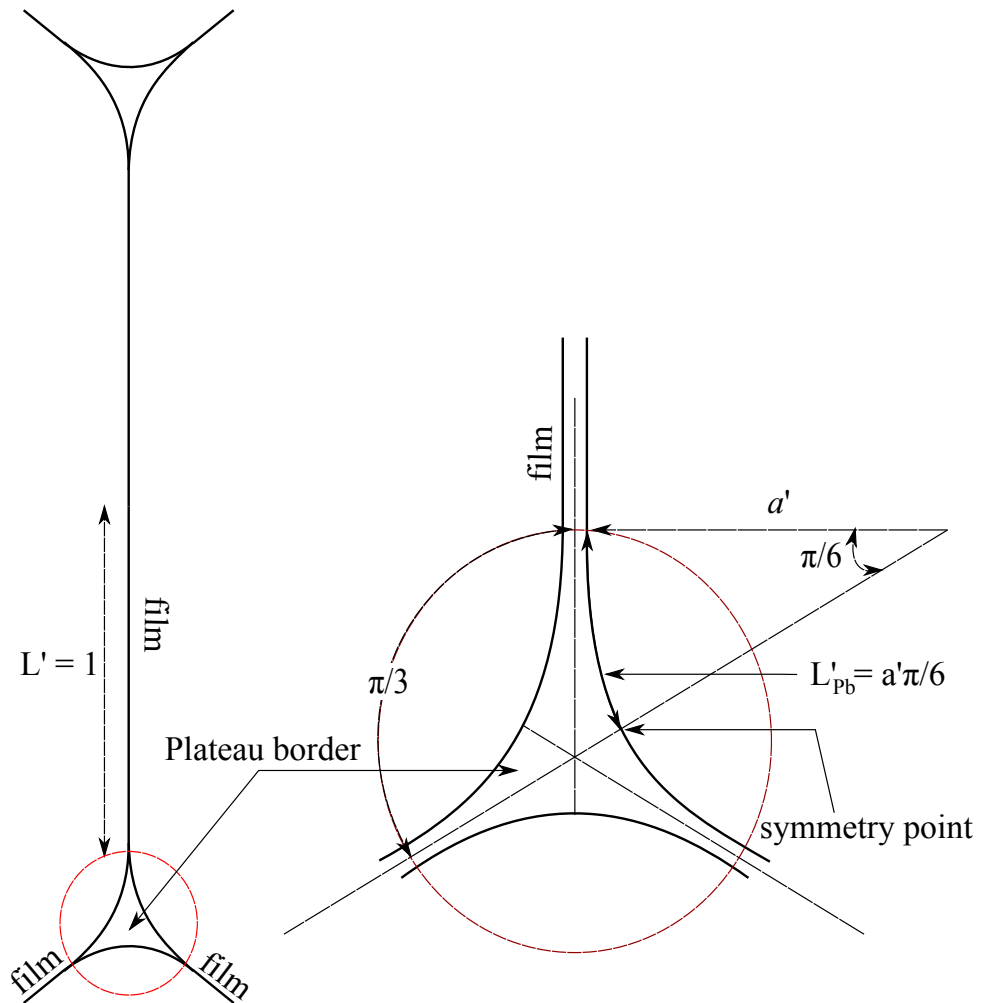


Figure 2: Illustration of half of a film and an adjacent Plateau border. The half-length of the film (L' in dimensionless variables) is set to unity. The zoomed view shows the cross section of the Plateau border. The total distance from the midpoint of the film to that of the Plateau border is $L' + L'_{pb} \equiv 1 + a'\pi/6$ where for the purpose of our model, we assume that the curved shape of the Plateau border surface can be ‘uncurled’ onto a straight line.

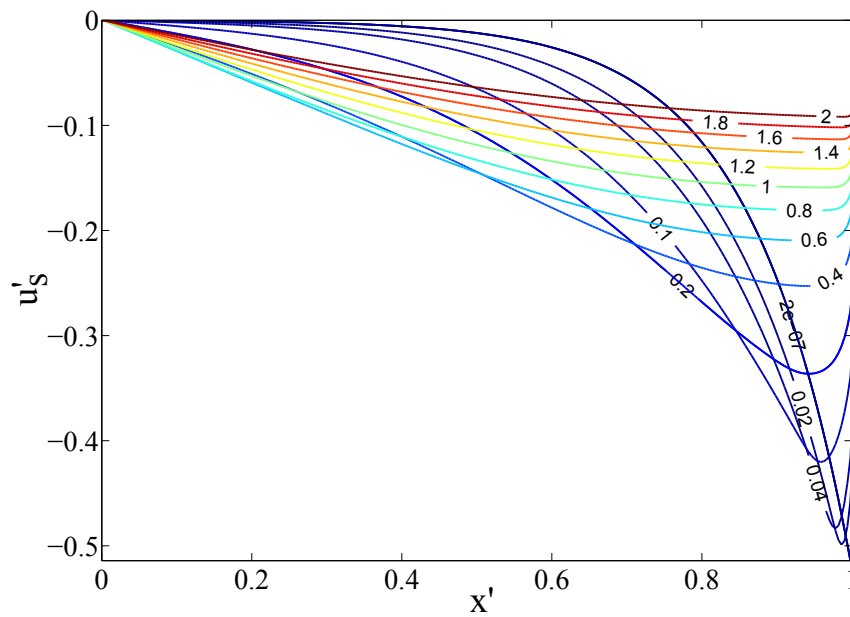


Figure 3: Evolution of surface velocity computed using $\delta'_0 \bar{\mu}_s = 5.4 \times 10^{-2}$ (obtained from $\delta'_0 = 6 \times 10^{-5}$ and $\bar{\mu}_s = 886$), $a' = 0.1$ and $\Gamma'_{F0} = 0.5$. The computation was carried out using the finite difference method. Labels on curves correspond to the time t' . At early times, the only significant surface velocities are seen in the region near the end of the film. At later times, the velocity profiles are more spread out, but the magnitude of the peak velocity is less.

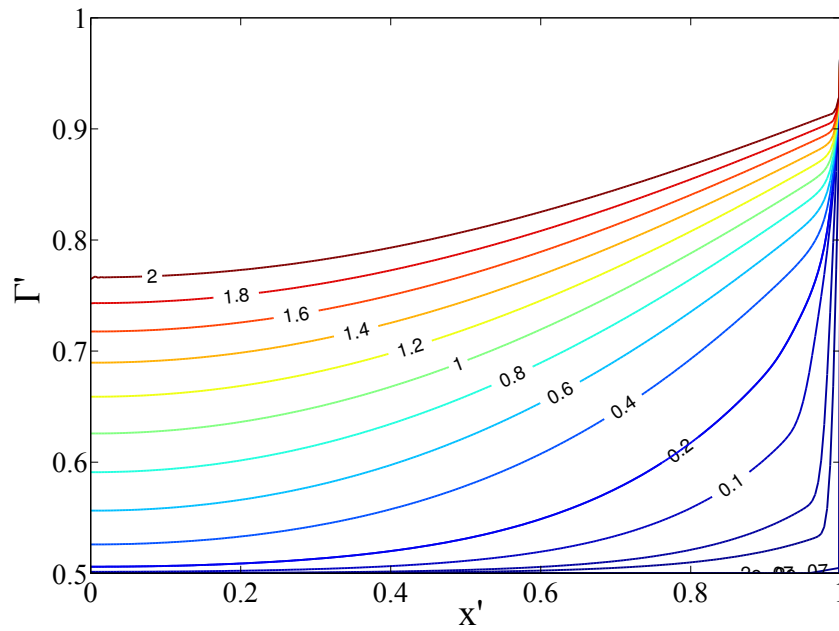


Figure 4: Evolution of surfactant surface concentration computed using $\delta'_0 \bar{\mu}_s = 5.4 \times 10^{-2}$ (obtained from $\delta'_0 = 6 \times 10^{-5}$ and $\bar{\mu}_s = 886$), $a' = 0.1$ and $\Gamma'_{F0} = 0.5$. The computation was carried out using the finite difference/material point method. Labels on curves correspond to the time t' . Surfactant accumulates on the film surface over time.

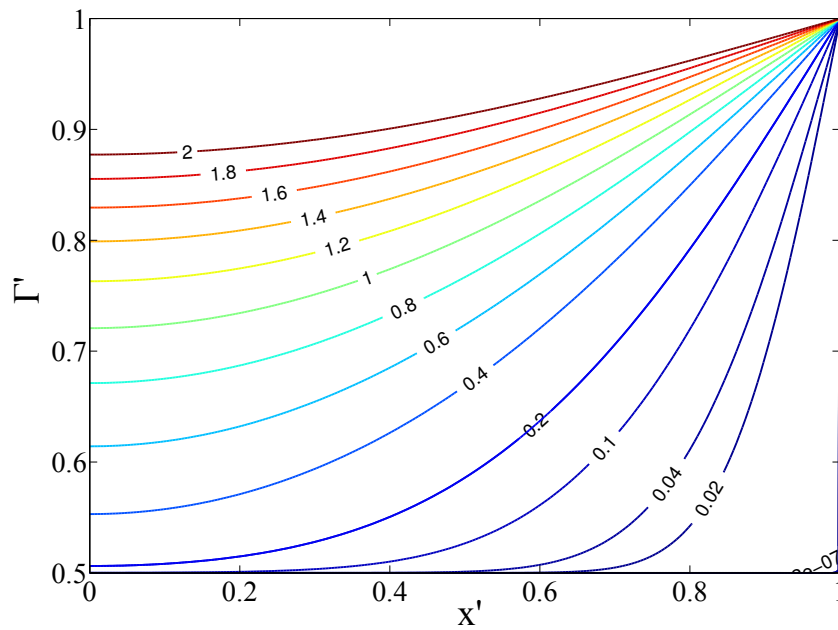


Figure 5: Evolution of surfactant surface concentration in the *absence* of surface viscosity simulated using $\delta'_0 = 6 \times 10^{-5}$, $\bar{\mu}_s = 0$, $a' = 0.1$ and $\Gamma'_{F0} = 0.5$. Labels on curves correspond to the time t' . Surfactant accumulates on the film surface over time more slowly in Figure 4 than it does here, owing to the surface viscosity affecting the results in Figure 4.

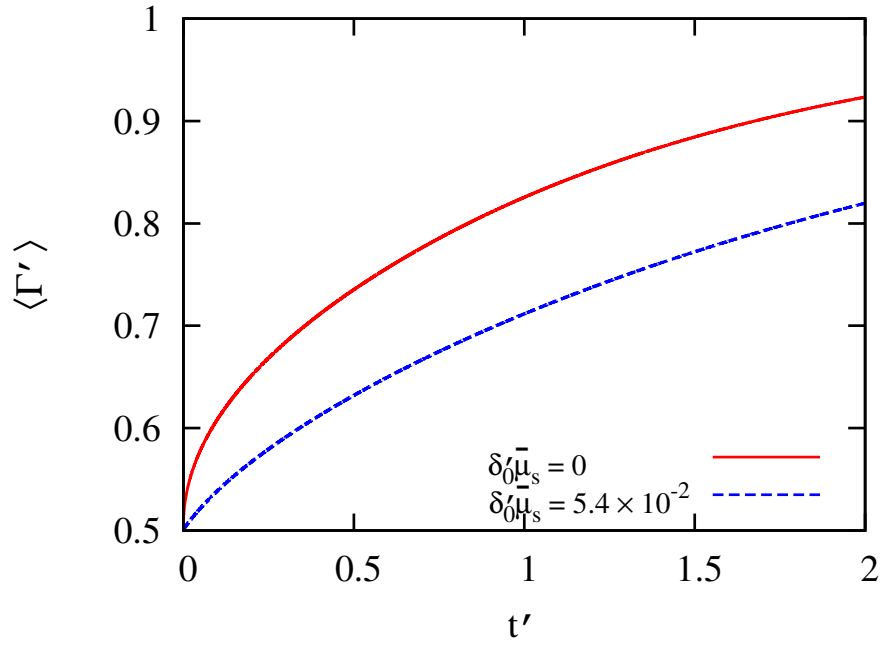


Figure 6: Comparison of the spatially-averaged surfactant surface concentration over time calculated without surface viscosity ($\delta'_0 \bar{\mu}_s = 0$, $\delta'_0 = 6 \times 10^{-5}$, $\bar{\mu}_s = 0$) and with surface viscosity ($\delta'_0 \bar{\mu}_s = 5.4 \times 10^{-2}$, $\delta'_0 = 6 \times 10^{-5}$, $\bar{\mu}_s = 886$). The computation used $a' = 0.1$ and $\Gamma'_{F0} = 0.5$. The computation was carried out using the finite difference method. Surface viscosity slows down the accumulation of surfactant.

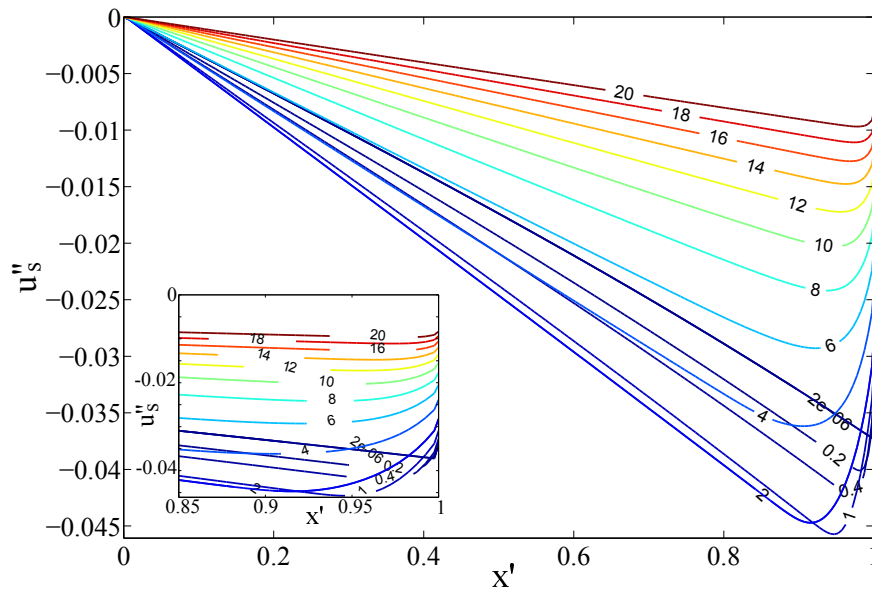


Figure 7: Evolution of surface velocity calculated using $\delta'_0 \bar{\mu}_s = 5.4$ (obtained from $\delta'_0 = 6 \times 10^{-5}$ and $\bar{\mu}_s = 8.86 \times 10^4$), $a' = 0.1$ and $\Gamma'_{F0} = 0.5$. The computation was carried out using the finite difference method. Labels on curves are the rescaled dimensionless time t'' . The inset is zoomed in around $x' = 1$. The velocity profiles show a linear variation with x' over much of the domain, but an abrupt deviation from linearity near $x' = 1$.

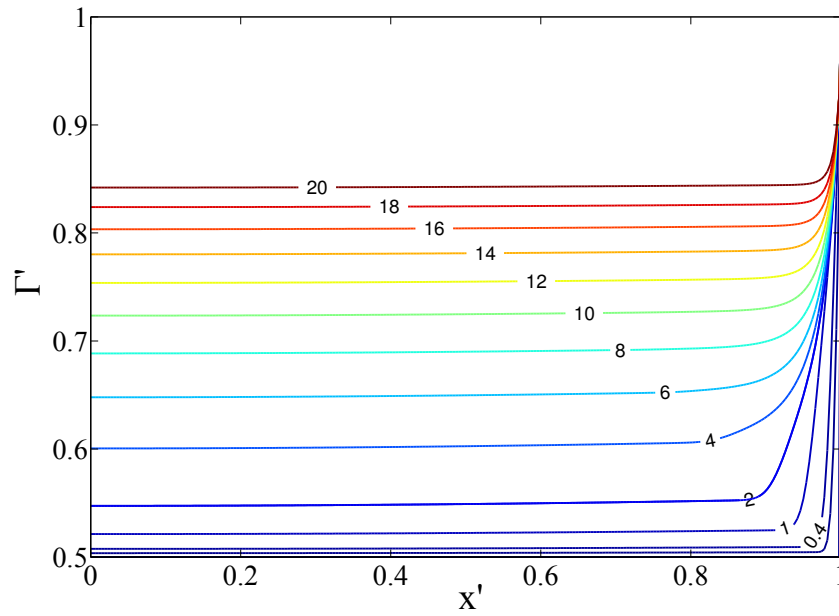


Figure 8: Evolution of surfactant surface concentration calculated using parameters $\delta'_0 \bar{\mu}_s = 5.4$ (obtained from $\delta'_0 = 6 \times 10^{-5}$ and $\bar{\mu}_s = 8.86 \times 10^4$), $a' = 0.1$ and $\Gamma'_{F0} = 0.5$. The computation was carried out using the finite difference/material point method. Labels on curves are the rescaled dimensionless time t'' . The profiles show a uniform concentration region over much of the domain with an abrupt change in concentration at the end of the domain.

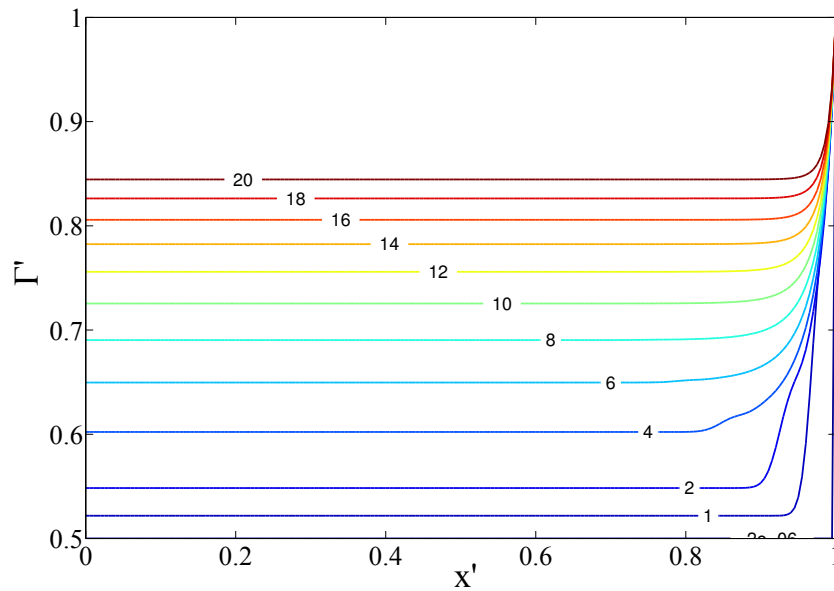


Figure 9: Evolution of surfactant surface concentration calculated with the integro-differential equation (as described in the appendix, and applicable for $\delta'_0 \bar{\mu}_s \rightarrow \infty$), using parameters $a' = 0.1$ and $\Gamma'_{F0} = 0.5$. Labels on curves are the rescaled dimensionless time t'' . Close agreement is seen between the integro-differential equation results here ($\delta'_0 \bar{\mu}_s \rightarrow \infty$) and the finite difference results (Figure 8 with $\delta'_0 \bar{\mu}_s = 5.4$).

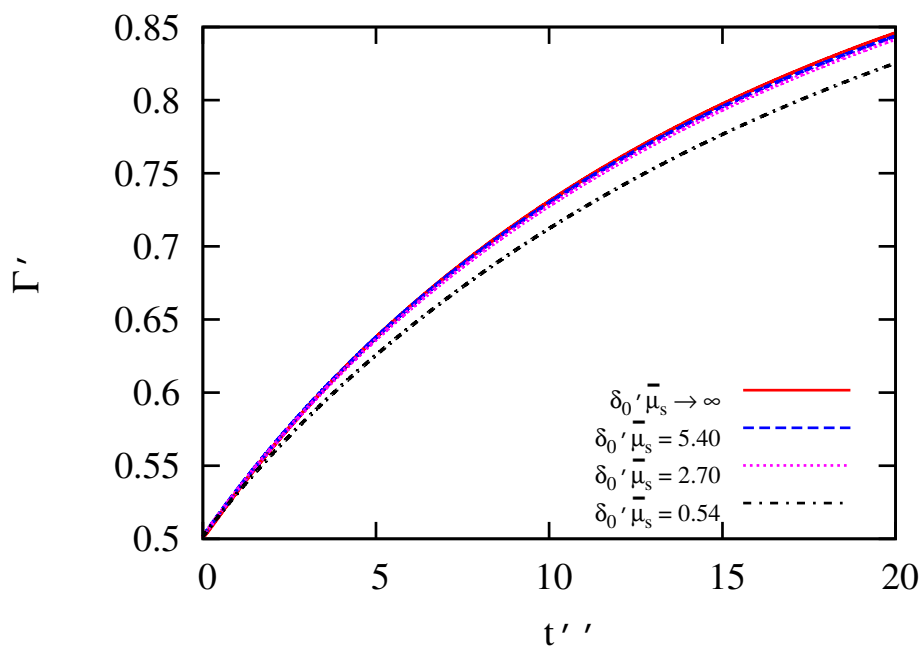


Figure 10: Comparison of the spatially-averaged surfactant surface concentration over time calculated using the integro-differential equation ($\delta'_0 \bar{\mu}_s \rightarrow \infty$) and the finite difference/material point method ($\delta'_0 = 6 \times 10^{-5}$, $\bar{\mu}_s = 8.86 \times 10^4$, $\delta'_0 \bar{\mu}_s = 5.4$) with additional data for $\delta'_0 \bar{\mu}_s = 2.7$ and 0.54 also included for comparison. All computations had $a' = 0.1$ and $\Gamma'_{F0} = 0.5$. Data for $\delta'_0 \bar{\mu}_s \rightarrow \infty$, $\delta'_0 \bar{\mu}_s = 5.4$ and $\delta'_0 \bar{\mu}_s = 2.7$ are difficult to distinguish on the scale of the plot. Differences start to appear as $\delta'_0 \bar{\mu}_s$ decreases, e.g. for the case $\delta'_0 \bar{\mu}_s = 0.54$.

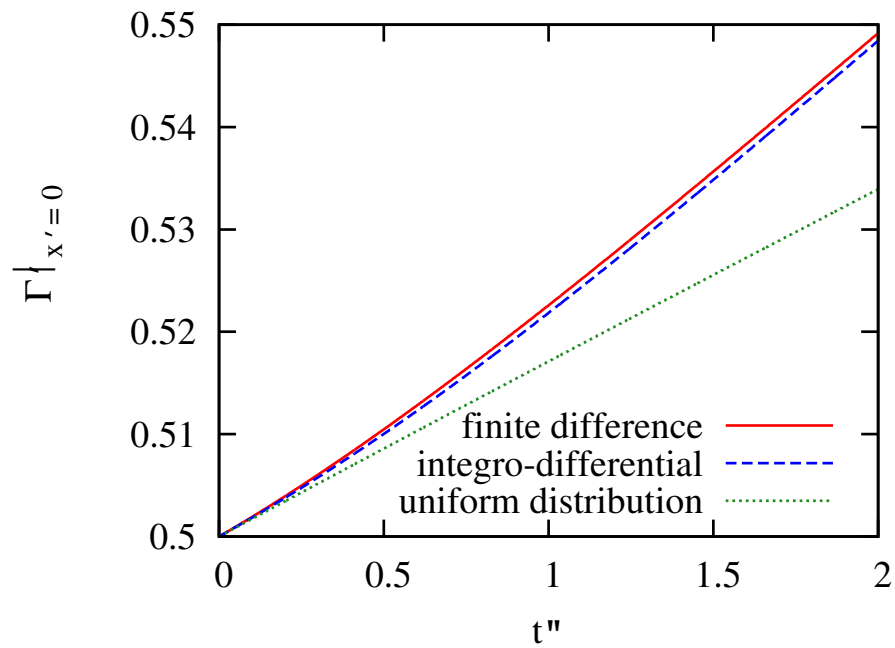


Figure 11: Comparison of the surfactant surface concentration (evaluated at $x' = 0$) vs time predicted using equation (A.10) (an analytic approximation assuming a near uniform surfactant distribution) and calculated using the finite difference/material point method ($\delta'_0 \bar{\mu}_s = 5.4$, $\delta'_0 = 6 \times 10^{-5}$, $\bar{\mu}_s = 8.86 \times 10^4$) and the integro-differential equation ($\delta'_0 \bar{\mu}_s \rightarrow \infty$). The computations had $a' = 0.1$ and $\Gamma'_{F0} = 0.5$. The predictions of equation (A.10) capture the qualitative behaviour.

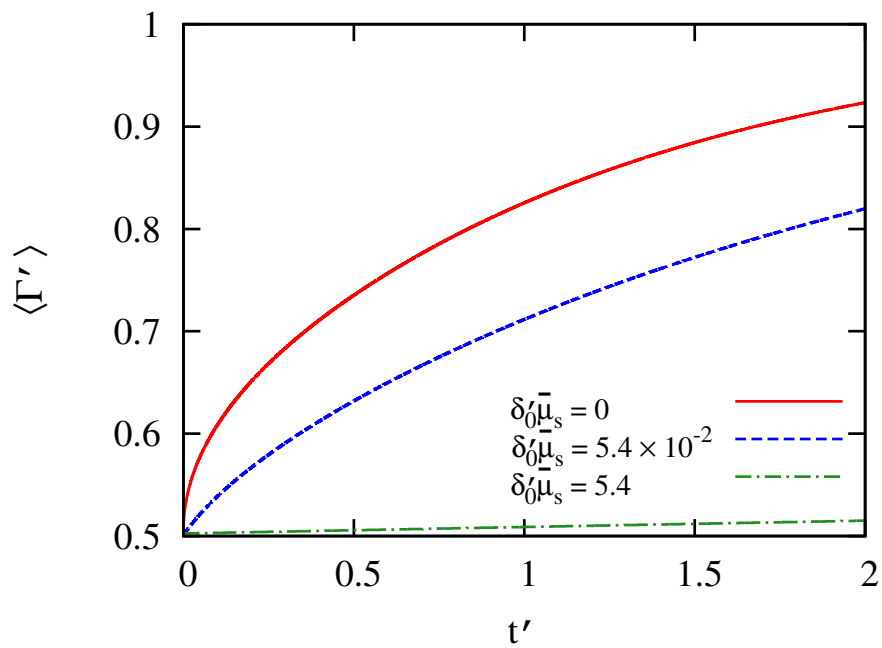


Figure 12: Comparison of the spatially-averaged surfactant surface concentration over time calculated in the absence of surface viscosity and in the presence of surface viscosity ($\delta'_0 \bar{\mu}_s = 0$ – 5.4 , $\bar{\mu}_s = 0$ – 8.86×10^4). The simulation used $\delta'_0 = 6 \times 10^{-5}$, $a' = 0.1$ and $\Gamma'_{F0} = 0.5$. Computations were carried out using the [finite difference/material point](#) method. High surface viscosity severely limits the rate at which surfactant accumulates on the film.

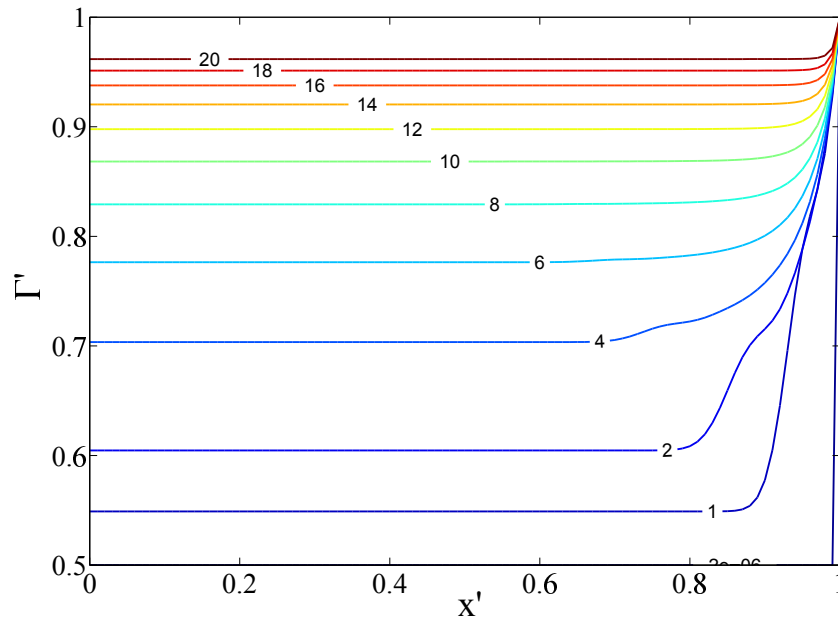


Figure 13: Evolution of surfactant surface concentration simulated using the integro-differential equation [as described in the appendix](#) (applicable in the limit $\delta'_0 \bar{\mu}_s \rightarrow \infty$) using parameters $a' = 0.25$ and $\Gamma'_{F0} = 0.5$. Labels on curves are the rescaled dimensionless time t'' . Evolution is more rapid here than in Figure 9, owing to the larger a' value used here.

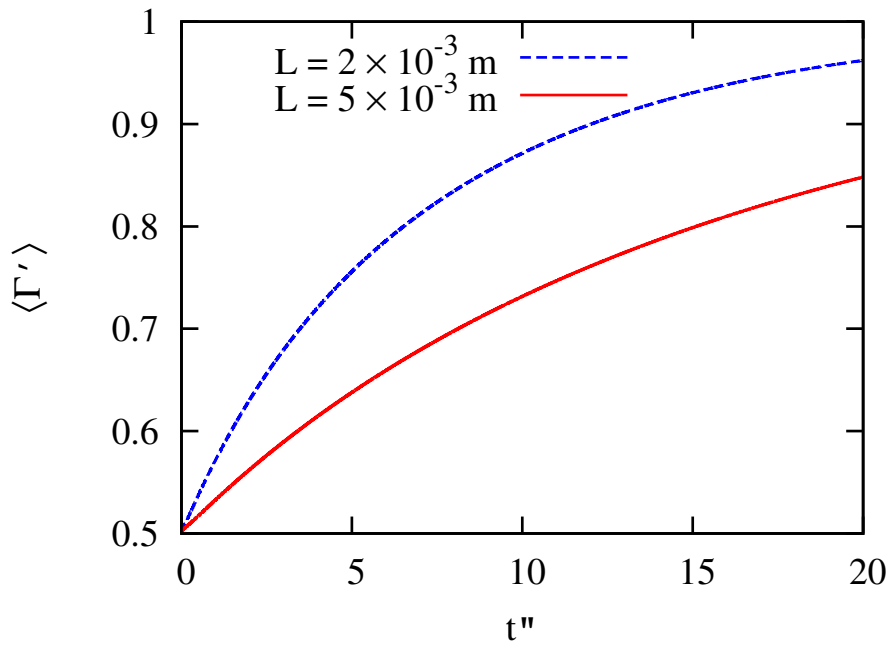


Figure 14: Comparison of the spatially-averaged surfactant surface concentration over time calculated using two different film lengths (i.e. two different a'). The computation used $L = 2 \times 10^{-3} \text{ m}$, corresponding to $a' = 0.25$, and $L = 5 \times 10^{-3} \text{ m}$, corresponding to $a' = 0.1$. In addition $\Gamma'_{F0} = 0.5$. The computational method used the integro-differential equation (applicable for $\delta'_0 \bar{\mu}_s \rightarrow \infty$). Faster surfactant accumulation is seen with smaller L , i.e. larger a' .